micromachines

MDPI

Review

Multiplex Detection in Label-Free Optical Biosensors: A Comparative Review of Seven Platforms

Maria Despoina Dipla [1,2], Dimitra Tsounidi [1], Ioannis Raptis [3], Eleni Rakanta [2], Konstantinos G. Beltsios [2,*] and Panagiota Petrou [1,*]

[1] Immunoassays/Immunosensors Lab, Institute of Nuclear and Radiological Sciences and Technology, Energy and Safety, NCSR "Demokritos", 15341 Aghia Paraskevi, Greece
[2] School of Chemical Engineering, National Technical University of Athens, 15780 Athens, Greece; erakanta@central.ntua.gr
[3] Institute of Nanoscience and Nanotechnology, NCSR "Demokritos", 15341 Aghia Paraskevi, Greece; i.raptis@inn.demokritos.gr
* Correspondence: kgbelt@mail.ntua.gr (K.G.B.); ypetrou@rrp.demokritos.gr (P.P.); Tel.: +30-2107723101 (K.G.B.); +30-2106503819 (P.P.)

Abstract

Optical biosensors are analytical platforms with widespread applications in biotechnology, environmental monitoring, food safety, and clinical diagnostics. Among these, label-free optical biosensing has attracted considerable research interest, driven by advances in nanotechnology and photonic integration, which have enabled the development of compact device architectures, enhanced analytical sensitivity, and robust multiplexed detection capabilities. By eliminating the need for labels, these techniques simplify sample preparation, minimize label-induced interference, and facilitate real-time monitoring of binding kinetics. Despite these advantages, label-free optical biosensing platforms differ substantially in terms of their geometries, fabrication requirements, fluidic integration, and surface functionalization strategies. These differences make it challenging to assess their suitability based solely on detection limits. A comprehensive evaluation must therefore consider not only analytical performance but also the engineering requirements and practical considerations that govern their implementation. This review examines seven complementary label-free optical biosensing platforms developed for multiplexed detection, with particular emphasis on their operating principles, analytical capabilities, and progress toward integrated point-of-care applications. Through a comparative analysis of their analytical performance and implementation requirements, this review highlights the key technical trade-offs that determine the suitability of each platform for different analytical applications.

Keywords: optical sensors; label-free detection; multiplex determinations; refractometric approaches; reflectometric approaches

Check for updates

Academic Editors: Indu Sharma and Vasudeva Reddy Minnam Reddy

Received: 19 October 2026
Revised: 16 November 2026
Accepted: 23 November 2026
Published: 26 November 2026

Copyright: © 2026 by the authors. Licensee MDPI, Basel, Switzerland. This article is an open access article distributed under the terms and conditions of the Creative Commons Attribution (CC BY) license.

1. Introduction

Optical biosensors represent an important class of analytical platforms, offering selective and sensitive detection across a wide range of applications, including biotechnology, environmental monitoring, food safety, and clinical diagnostics [1–5]. Within this field, label-free optical biosensing has attracted considerable research interest, as advances in nanotechnology and photonic integration have enabled enhanced analytical sensitivity, compact device architectures and multiplexed detection capabilities [6]. Label-free approaches are particularly valuable for analysis of biomolecular interactions because they minimize

sample-preparation requirements, eliminate the need to modify binding molecules with labels, and enable the direct monitoring of binding kinetics [7]. These advances have facilitated the development of diverse optical transduction strategies, in which biomolecular binding events are translated into measurable changes in optical properties such as refractive index, phase, polarization or optical thickness [6–8].

Direct label-free optical transduction can be broadly classified into two main categories: refractometric and reflectometric approaches (Figure 1). In refractometric systems, biomolecular binding induces changes in the local refractive index, which are detected through the interaction of the analyte with an evanescent optical field. In waveguide-based interferometers, for instance, these refractive index changes alter the phase of the guided optical mode relative to a reference field, thereby generating a measurable interference signal [6–9]. Reflectometric approaches, by contrast, rely on multiple reflections within layered optical structures. In these systems, variations in the refractive index and physical thickness of individual layers alter the optical thickness (n·d), consequently modifying the resulting interference pattern [7].

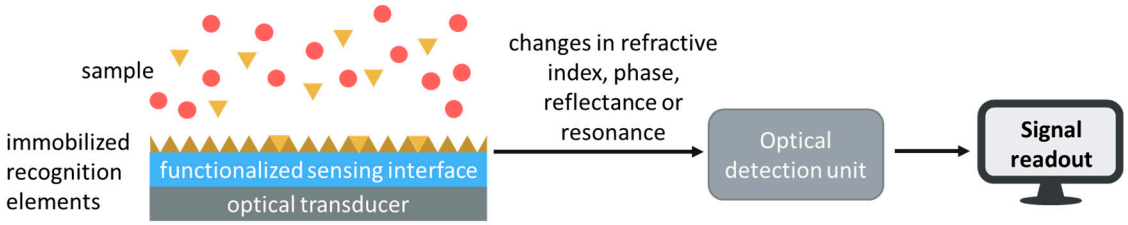

Figure 1. General schematic of label-free optical biosensing. The binding of target analyte to immobilized recognition elements on the functionalized sensing surface induces changes in the optical properties of the transducer. These changes are detected and converted into a measurable signal, enabling the label-free detection of target molecules.

Despite sharing the common principle of label-free optical detection, optical biosensor architectures differ considerably in terms of sensing geometry, optical interrogation methods, fabrication requirements, fluidic integration, and surface biofunctionalization. These design considerations influence not only analytical performance, but also the complexity, cost, reliability and integration potential of the resulting sensing platforms [10]. Consequently, comparisons based solely on individual performance metrics, such as detection limits, may provide an incomplete picture of their overall capabilities. Indeed, biosensor performance and practical application are also influenced by factors such as assay configuration, surface properties, operational simplicity, and the specific requirements of the intended application [7]. A meaningful evaluation of these technologies must therefore consider both their analytical performance and the broader engineering characteristics that govern their practical implementation.

In this context, the present review examines seven selected label-free optical biosensing platforms that represent complementary reflectometric, interferometric and plasmonic approaches: Reflectometric Interference Spectroscopy (RIfS), White Light Reflectance Spectroscopy (WLRS), Arrayed Imaging Reflectometry (AIR), Interferometric Reflectance Imaging Sensor (IRIS), Mach–Zehnder Interferometers (MZIs), Bimodal Interferometers (BiMW), and Surface Plasmon Resonance/Surface Plasmon Resonance Imaging (SPR/SPRi). These platforms were selected based on their relevance to multiplexed label-free detection and their potential for integration into practical analytical systems. The selection criteria included their underlying optical transduction mechanisms, demonstrated multiplexing capabilities, analytical performance, fabrication complexity, compatibility with microfluidic systems, surface functionalization requirements, and potential for point-of-care applica-

tions. Together, these technologies provide a representative basis for comparing different approaches to label-free optical biosensing and assessing the trade-offs between analytical performance and practical implementation. The selection of studies for this review was based on the underlying optical transduction mechanism rather than exclusively on the biochemical configuration of the assay. Studies were considered relevant when the optical transducer detected biomolecular interactions through changes in intrinsic optical properties, without relying on fluorescent, luminescent, or other optically active reporter labels as the primary detection mechanism. Studies incorporating secondary antibodies, biotin–streptavidin interactions, or enzymatic amplification were also considered when these steps were used to enhance analyte capture or signal generation while retaining an optical transduction mechanism based on changes in the sensing interface.

2. State-of-the-Art of Multiplexed Optical Label-Free Biosensors

2.1. Reflectometric Interference Spectroscopy (RIfS)

Reflectometric Interference Spectroscopy (RIfS) is a label-free optical sensing technique based on white-light interference in transparent thin-film structures (Figure 2a). At each interface between layers with different refractive indices, incident light is partially reflected and transmitted. The reflected beams subsequently interfere, generating a wavelength-dependent interference spectrum. The positions of the spectral peaks depend on the optical thickness of the sensing layer, which is determined by its refractive index and physical thickness, as well as on the angle of light incidence and the refractive index of the surrounding medium. Upon biomolecular binding to the functionalized sensor surface, the optical thickness of the upper sensing region increases, resulting in a shift in the interference spectrum. Monitoring this spectral shift over time enables the label-free, time-resolved analysis of molecular association and dissociation processes [11].

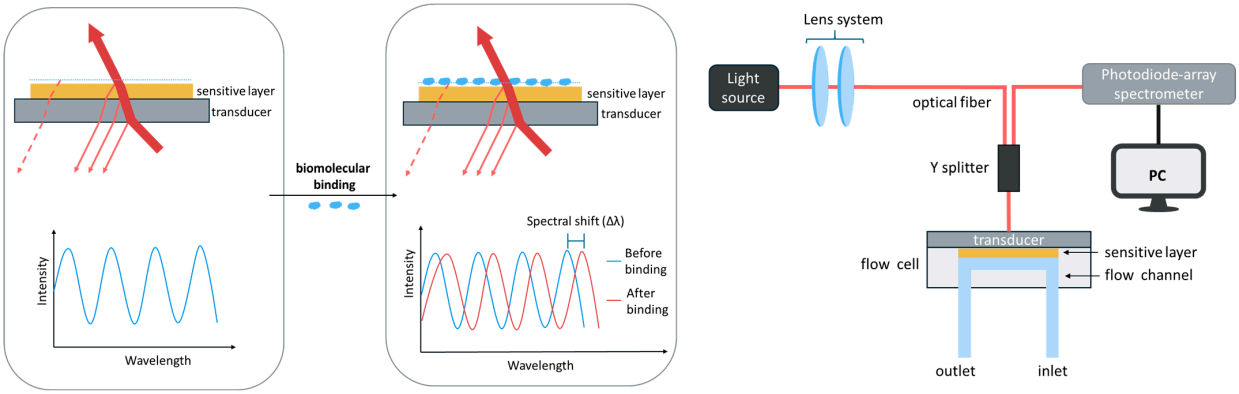

Figure 2. (**a**) Schematic representation of signal generation in RIfS. Biomolecular binding at the sensing surface alters the optical thickness of the sensitive layer, resulting in a shift in the interference spectrum. Upward arrow represents the incident light whereas downward ones the light reflected at the interfaces of the layers consisting the sensing element. (**b**) Schematic representation of a conventional RIfS setup, comprising a broadband light source, a bifurcated optical fiber, a flow-cell transducer, a spectrometer, and a computer for signal acquisition and processing.

A conventional RIfS setup typically comprises a broadband white-light source, a bifurcated optical fiber, a thin-film transducer mounted in a microfluidic flow cell, and a spectrometer for spectral detection (Figure 2b). White light is guided through one branch of the fiber to the rear side of the transducer, while the reflected light is collected through the same optical path and directed through the second branch to an ultra-violet/visible (UV/vis) diode-array spectrometer. Halogen lamps or light-emitting diodes (LEDs) can

both serve as excitation sources. Standard RIfS transducers commonly consist of a glass substrate coated with a high-refractive-index layer, such as Ta_2O_5 or Nb_2O_5, topped with a SiO_2 layer that can be further functionalized to enable immobilization of biorecognition molecules and suppression of nonspecific adsorption [11,12]. Recent studies have also explored alternative sensing architectures, including nanoporous anodic alumina structures for biomolecular monitoring [13].

Multiplexing in RIfS has been achieved through different optical and spatial interrogation strategies. Polarized imaging reflectometric interference spectroscopy (pi-RIfS) introduced a spatially resolved route to multiplexed RIfS by combining antigen microarrays with imaging-based detection. Bleher et al. [14] demonstrated the parallel, label-free monitoring of three antiphospholipid-syndrome-related antigen–antibody interactions using β2-glycoprotein I, prothrombin, and cardiolipin immobilized on a single transducer. The platform employed a BK7 glass transducer coated with Ta_2O_5 and SiO_2, mounted in a polydimethylsiloxane (PDMS) flow cell and interrogated with a 470 nm coaxial LED, a polarization filter, telecentric optics and a camera. For surface functionalization, the glass surface was modified with 11-amino-undecyltrimethoxysilane (11-AUTMS), followed by conversion to a carboxyl-terminated layer. The surface was subsequently activated using N-hydroxysuccinimide (NHS) and diisopropyl-carbodiimide (DIC) chemistry to enable the covalent immobilization of β2-glycoprotein I, prothrombin and an amino-functionalized cardiolipin analog. The resulting antigen microarray enabled the simultaneous label-free detection of the corresponding autoantibodies in purified human serum samples. In a proof-of-principle clinical evaluation involving three patients with antiphospholipid syndrome and three healthy controls, the responses obtained for β2-glycoprotein I and cardiolipin clearly distinguished from negative samples. The platform enabled parallel monitoring of all three antigen–antibody interactions within approximately 10 min, demonstrating its potential for rapid multiplexed autoantibody profiling using pi-RIfS [14].

The clinical evaluation of the pi-RIfS microarray was subsequently extended to a larger cohort and an expanded four-antigen panel. The array comprised β2-glycoprotein I, prothrombin, cardiolipin and a β2-glycoprotein I/cardiolipin complex, together with bovine serum albumin (BSA) control spots, immobilized on 11-AUTMS-modified glass transducers. Prior to analysis, serum immunoglobulins G (IgG) fractions were purified to reduce nonspecific matrix interactions, and each antigen was represented by three replicate spots. The study included samples from 35 patients with antiphospholipid syndrome, six patients with systemic lupus erythematosus, and 24 healthy controls. All four antigen–antibody interactions were monitored simultaneously on a single chip, with coefficients of variation below 5% in more than 95% of measurements. Depending on the antigen, clinical sensitivity ranged from 0.800 to 0.929, while clinical specificity ranged from 0.733 to 0.969, with β2-glycoprotein I and prothrombin showing the best overall performance. All four serological parameters were determined within approximately 10 min, and the results showed good agreement with the respective enzyme-linked immunosorbent assays (ELISA) [15].

A simplified RIfS format, 1-λ reflectometry, adopted a different multiplexing strategy by monitoring binding-induced changes in reflected light intensity at a single wavelength. Its portable detection module incorporated a 470 nm LED, confocal optics and an integrated photodiode. A movable x–y stage sequentially positioned different sensing regions of the same transducer beneath the detector, enabling time-resolved interrogation without the need for imaging. The glass transducers consisted of BK7 glass coated with Ta_2O_5 and SiO_2 and were modified with 3-glycidyloxypropyltrimethoxysilane (GOPTS) and aminodextran. For anti-*Salmonella* antibody detection, *Salmonella* lipopolysaccharides were immobilized through hydrophobic interaction involving decane residues, whereas anti-C-reactive pro-

tein (CRP) antibodies were covalently immobilized through amine-coupling chemistry. Following assay optimization, both assays were transferred from single-spot to two-spot measurements, permitting simultaneous label-free determination of anti-*Salmonella* antibodies and CRP in the same sample. The minimum detectable concentrations were 1.56 mg/L for anti-*Salmonella* antibodies and 0.51 mg/L for CRP, with corresponding working ranges of 5.74–122.52 and 1.26–29.56 mg/L, respectively. These values were comparable to those obtained with the corresponding single-spot assays, with slightly improved performance for CRP. Moreover, measurements using sera from *Salmonella*-infected chickens successfully distinguished antibody-positive from antibody-negative samples and differentiated responses to *S. typhimurium* and *S. enteritidis* [16].

More recently, RIfS and 1-λ reflectometry have been used to investigate kinase–inhibitor interactions and characterize their binding kinetics. Initial RIfS measurements monitored, in real time, the binding of kinases to surface-immobilized inhibitors through changes in optical thickness. The resulting binding curves were used to estimate association and dissociation rate constants, as well as dissociation constants for individual kinase–inhibitor pairs. The sensor surface was functionalized with GOPTS and aminodextran, followed by glutaric-anhydride treatment and NHS/DIC activation to enable covalent immobilization of the inhibitors. The aminodextran layer helped to minimize nonspecific adsorption. The approach was subsequently transferred to an imaging-based 1-λ reflectometry configuration, employing 535 nm LED illumination and CCD-based detection to monitor arrays of inhibitor spots on a single transducer. Automatic spotting enabled the preparation of a 5 × 7 array containing different inhibitors, including staurosporine, fasudil, imatinib and two molecular fragments, arranged in rows for parallel investigation of kinase–inhibitor interactions. The resulting binding curves provided both qualitative screening information and quantitative kinetic and affinity data, demonstrating the potential of this platform for both kinase and inhibitor screening [17].

Taken together, these studies demonstrate that multiplexing in RIfS can be achieved through distinct optical and spatial interrogation architectures, each addressing different analytical requirements. Imaging-based pi-RIfS enables genuinely parallel spatial readout and has progressed from proof-of-principle autoantibody profiling to evaluation in a larger clinical cohort, although it requires imaging optics and camera-based detection. In contrast, movable-stage 1-λ reflectometry replaces simultaneous imaging with sequential interrogation of spatially separated sensing regions. This approach reduces optical complexity and supports the development of compact, portable point-of-need systems while retaining the ability to analyze multiple targets in the same sample. Thus, the choice of multiplexing architecture depends not only on the number of interactions that can be monitored, but also on the desired degree of parallelization, instrumentation complexity, portability, level of clinical validation, and type of analytical information required.

2.2. White Light Reflectance Spectroscopy (WLRS)

White Light Reflectance Spectroscopy (WLRS) is a label-free optical sensing technique based on broadband light interference in layered sensing structures. When light reaches the sensing surface, it is partially reflected at the different interfaces. These reflected beams interfere with one another, generating a characteristic reflectance spectrum. The position and shape of the interference fringes depend on the refractive indices and thicknesses of the individual layers. Biomolecular binding to the functionalized surface leads to the formation and gradual growth of a biomolecular adlayer. As the optical thickness of this layer increases, the interference spectrum shifts. Real-time monitoring of these shifts makes it possible to track biomolecular layer growth and correlate it with analyte concentration, thereby enabling the quantitative, label-free detection of biomolecular interactions [18,19].

The standard WLRS biosensing arrangement consists of a broadband white-light source, a reflection probe, a SiO_2/Si sensing chip and a spectrometer (Figure 3a). The probe contains seven optical fibers: six peripheral fibers deliver light vertically onto the sensing surface, while the central fiber collects the reflected light and directs it to the spectrometer. The sensing element is a silicon substrate covered with a thermally grown SiO_2 layer, on which the biomolecular recognition layer is formed. During the assay, the chip is placed in a microfluidic cell to enable the controlled delivery of samples and reagents. The collected reflectance spectrum is fitted to the theoretical interference spectrum using a Levenberg–Marquardt algorithm. This approach enables real-time monitoring of changes in biomolecular adlayer thickness with sub-Ångström resolution (Figure 3b) [18,19].

WLRS has been applied to a range of single-analyte assays demonstrating its applicability to clinical, food-safety and microbial analysis [18,19]. Multiplexed WLRS was first implemented through the spatial patterning of distinct recognition regions on the same SiO_2/Si chip combined with mechanical scanning of the sensing surface relative to a fixed reflection probe. The approach was demonstrated by the simultaneous determination of CRP and D-dimer in human plasma samples with biochips modified with distinct bands of anti-CRP and anti-D-dimer specific antibodies. The biochip was mounted on a computer-controlled X–Y stage. Prior to antibody spotting, the chips were cleaned and hydrophilized using Piranha solution and functionalized with 3-amino-propyltriethoxysilane (APTES). CRP was detected directly, whereas D-dimer was determined using a two-step sandwich immunoassay involving a biotinylated reporter antibody and streptavidin. Both analytes exhibited detection limits of 25 μg/L. Evaluation of 35 human plasma samples demonstrated excellent agreement with standard diagnostic laboratory methods, yielding R^2 values of 0.997 for CRP and 0.998 for D-dimer. Although demonstrated for two biomarkers, the same platform could accommodate and successfully interrogate up to seven antibody bands on a single sensing surface, highlighting its potential for higher-order multiplexing [20].

The same approach was subsequently applied for the simultaneous determination of paraquat and atrazine pesticides in bottled and tap water samples (Figure 3c) [21]. The SiO_2/Si chip contained two spatially distinct sensing bands functionalized with paraquat–BSA and atrazine–BSA conjugates, respectively. The two regions were sequentially interrogated by moving the chip relative to the reflection probe using a linear stage. A competitive immunoassay was performed by incubating samples or calibrators with both analyte-specific antibodies, followed by signal enhancement using a secondary antibody. Detection limits of 40 ng/L for paraquat and 50 ng/L for atrazine were achieved, with corresponding working ranges of 0.08–2.5 and 0.10–5.0 μg/L, respectively. Furthermore, the biochip could also be regenerated with 0.5% SDS and reused for at least 20 assay cycles [21].

A different multiplexing strategy was introduced by Anastasiadis et al. [22] to eliminate the need for mechanical scanning, namely Multi-Area Reflectance Spectroscopy (MARS). In this approach, the Si chip incorporated two adjacent sensing areas with different SiO_2 thicknesses, each functionalized with a distinct mycotoxin–protein conjugate. A single fixed reflection probe simultaneously interrogated both areas, while the resulting reflectance spectrum was mathematically deconvoluted to independently determine the effective biomolecular adlayer thickness at each sensing region. Using this configuration, aflatoxin B1 and fumonisin B1 were simultaneously determined through a competitive immunoassay, achieving detection limits of 0.05 and 1.0 μg/L, respectively, and dynamic ranges of 0.1–5.0 and 2.0–50 μg/L. The assay was completed within 12 min and validated with wheat and maize samples following an optimized extraction protocol, with recoveries between 85 and 115% [22].

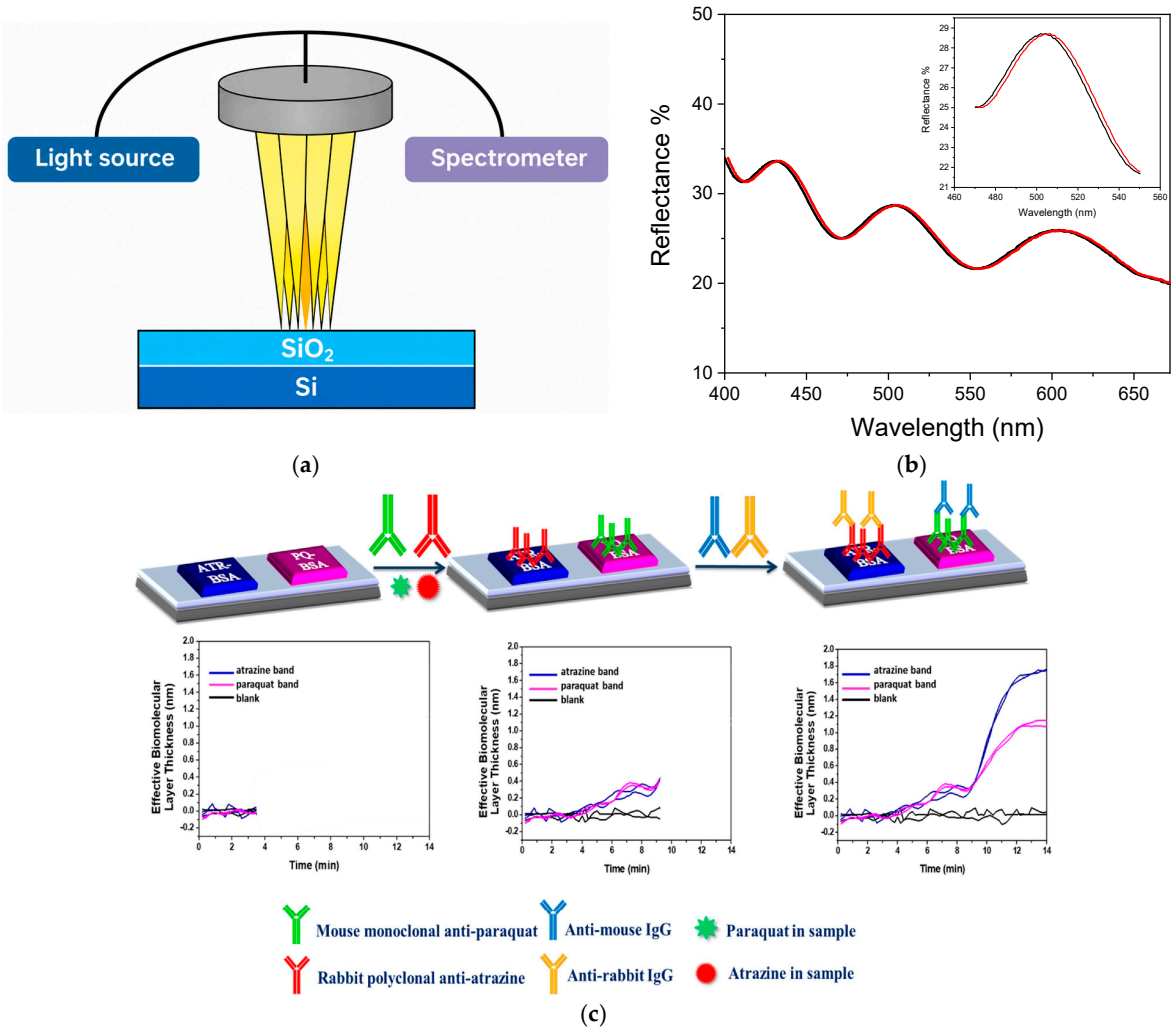

Figure 3. White Light Reflectance Spectroscopy (WLRS). (**a**) Schematic representation of a conventional WLRS setup, comprising a broadband light source and a reflection probe used to interrogate a Si/SiO_2 sensing chip. (**b**) Representative reflectance spectrum showing the wavelength-dependent interference pattern and its shift following biomolecular binding. Black line: reflectance spectrum prior to reaction; Red line: reflectance spectrum after the reaction. (**c**) Schematic of the dual-analyte biochip and the competitive assay format followed for the simultaneous determination of atrazine and paraquat (upper part). Indicative biomolecular adlayer thickness change during the different steps of the dual-analyte assay depicted at the top part of the figure (lower part) [21].

In summary, two distinct approaches to multi-analyte detection based on the WLRS detection principle have been reported. The first relies on spatially patterned recognition regions on a single chip combined with mechanical scanning. This strategy offers flexibility in the arrangement of multiple sensing regions and has been successfully demonstrated in both clinical and environmental applications. However, it requires controlled movement of the chip relative to the optical probe. In contrast, MARS enables the simultaneous interrogation of multiple sensing regions using a fixed optical configuration, relying on spectral separation and computational deconvolution to distinguish the individual responses. This eliminates the need for mechanical scanning and reduces instrumental complexity. Importantly, both approaches retain the label-free nature of optical transduction, although reporter antibodies or secondary-antibody amplification are used in some assays to enhance analytical sensitivity. Overall, the main differences between these multiplexing strategies lie in their approach to spatial interrogation, instrumentation requirements,

need for assay amplification, and potential for integration into portable and point-of-need analytical systems.

2.3. Arrayed Imaging Reflectometry (AIR)

Arrayed Imaging Reflectometry (AIR) is a label-free optical biosensing technique that relies on thin-film interference. The sensing surface consists of a silicon substrate coated with a thin silicon dioxide layer and functionalized with immobilized capture probes. The optical properties of the substrate and coating are carefully optimized to establish a near-total destructive interference condition, under which the reflected intensity approaches zero in the absence of target binding. Upon binding of analyte molecules to the immobilized probes, the optical thickness of the surface layer increases, perturbing this antireflective condition and resulting in a measurable increase in reflected intensity. Following calibration, the measured reflectance can be correlated with changes in surface-layer thickness and, ultimately, with analyte concentration, enabling label-free detection and quantification of biomolecular interactions [23,24].

A typical AIR setup consists of a linearly polarized light source, beam-conditioning optics, a Si/SiO_2 sensor chip, and a CCD camera for imaging the reflected light (Figure 4a). In the conventional configuration, a HeNe laser operating at 632.8 nm is linearly polarized to a high s polarization ratio, spatially filtered, expanded, and collimated before illuminating the sensor surface at an incidence angle of 70.6°, which minimizes reflectance by the SiO_2/Si chip. The sensor surface is chemically functionalized with capture probes arranged in a microarray format. The thicknesses of the SiO_2 and adhesion chemistry layers are selected to establish the near-antireflective condition following probe immobilization. A CCD camera captures the light reflected from the entire sensing area, allowing multiple capture spots to be imaged simultaneously. The resulting pixel intensities can be converted into changes in surface-layer thickness, enabling spatially resolved measurements of binding events across the microarray and providing the basis for multiplexed biomolecular analysis [23,24].

AIR has demonstrated multiplexing since its early applications through spatially resolved microarray imaging. One of the early multiplexed AIR applications targeted five cytokines: IL-5, IL-8, IL-12, IFN-γ and TNF-α, using an antibody array. Mace et al. functionalized SiO_2/Si chips with APTES and glutaraldehyde, followed by the covalent immobilization of capture antibodies in an array format and subsequent BSA blocking [23]. Selective detection of TNF-α and IFN-γ was initially demonstrated at 1 mg/L, with negligible responses from non-target probe spots. IL-5 was subsequently added at 500 µg/L, increasing the number of simultaneously detected cytokines to three. In a separate sensitivity study, IFN-γ could be clearly detected down to 250 ng/L [25]. The multiplexing capacity of AIR was subsequently extended to a 14-analyte microarray comprising cytokines and other inflammatory biomarkers. Antibodies were covalently immobilized as approximately 100 µm spots on APTES/glutaraldehyde-functionalized SiO_2/Si chips. Depending on the analyte, the limits of detection ranged from 1 to 100 ng/L, while Tissue Factor (TF) was detected at concentrations below 1 ng/L. Most assays also exhibited dynamic ranges spanning approximately five orders of magnitude. Measurements of mixtures containing at least two analytes closely matched the corresponding singleplex results, with correlation values ranging from 85.2 to 97.1% across the 14-analyte panel. The assays were performed in buffered BSA and diluted bovine serum, and IFN-γ could additionally be detected in 20% bovine serum with a detection limit of 10 ng/L [25].

AIR was also adapted to multiplexed influenza serology using a hemagglutinin microarray containing 16 recombinant antigens representing influenza A subtypes H1-H12 and influenza B. The hemagglutinins were printed on amine-reactive AIR substrates using a piezoelectric non-contact microarray spotter, typically in ten replicate spots per antigen,

alongside positive and negative controls. The arrays were subsequently blocked with BSA. Serum samples from experimentally infected and field-collected mallards were used to evaluate the platform. In challenge experiments involving H3, H4, H6 and H12 influenza viruses, the array generally produced strong subtype-specific antibody responses, with detection extending to serum dilutions of at least 1:100 for most strongly responding samples. In a further study of 13 field-collected mallard serum samples, multiplexed antibody profiles were generated and compared with microneutralization and virus-isolation results. In most cases, the AIR-derived profiles were consistent with the serological profiles obtained using conventional methods [26].

Human autoantibody profiling provided another application of multiplexed AIR serology. A five-plex array comprising Ro60, La/SSB, Scl-70, BicD2, and Ro52 was prepared on amine-reactive AIR substrates with the autoantigens deposited using a piezoelectric non-contact microarray spotter, with six replicate spots per antigen, after which the remaining reactive surface was blocked. Initial testing with commercial polyclonal antibodies yielded antigen-specific limits of detection ranging from 8.36 to 68.56 μg/L. The platform was subsequently evaluated using five positive reference samples and ten human donor serum samples, enabling the simultaneous detection of autoantibodies against multiple antigens. The multiplex AIR measurements showed good agreement with corresponding singleplex ELISA and multiplex Luminex results [27].

Klose and Miller [28] explored another aspect of AIR multiplexing by combining different classes of recognition elements on the same sensing surface. An amine-reactive AIR substrate was modified with a mixture of amine-PEG11-biotin and amine-PEG4-methyl, followed by streptavidin immobilization and stabilization of the biotin–streptavidin layer with commercially available stabilization reagent (Stabil™Coat Plus Stabilizer). This common attachment strategy enabled the immobilization of both biotinylated aptamers and protein probes within the same microarray. Aptamer arrays targeting thrombin and TGF-β1 enabled the label-free detection of these two proteins with minimal cross-reactivity, yielding limits of detection of 12.7 and 74.5 μg/L, respectively, at a probe concentration of 100 μM. The strategy was subsequently extended to mixed aptamer-protein arrays, demonstrating the compatibility of different classes of recognition elements for immobilization on a single AIR sensing surface [28].

A 15-plex AIR microarray was also developed to profile antibody responses against SARS-CoV-2 and other respiratory viruses. The array contained 14 viral antigen probes representing SARS-CoV-2, SARS-CoV-1, MERS-CoV, three endemic human coronaviruses (HKU1, 229E and OC43), and three influenza strains. Antigens were printed in six replicate spots on amine-reactive silicon oxide substrates using a piezoelectric microarray spotter, followed by BSA passivation and additional blocking with fetal bovine serum to reduce nonspecific binding from human serum. Initial characterization with a commercial anti-SARS-CoV-2 polyclonal antibody yielded provisional limits of detection of 43.3 μg/L for S1+S2 ECD, 40.7 μg/L for S1, and 25.1 μg/L for RBD SARS-CoV-2 protein. Serum samples from 15 convalescent COVID-19 patients were subsequently analyzed, with S2- and RBD-specific responses showing statistically significant discrimination between COVID-19 positive and negative samples. Primary antibody binding was measured directly, while subsequent incubation with anti-human IgG or anti-human IgM antibodies enabled the identification of isotype-specific components of the antibody response [29].

An eight-antigen StaphAIR microarray was also developed for *Staphylococcus aureus* serology, using the IsdA, IsdB, IsdH, Gmd, Amd, CHIPS, SCIN, and Hla as antigens. These antigens were covalently immobilized by microarray spotting onto SiO_2/Si AIR chips bearing an amine-reactive surface. IsdA and SCIN were pre-incubated with streptavidin and avidin, respectively, to improve antigen deposition and preserve antigenicity. Following spotting,

the chips were blocked with BSA and fetal bovine serum and stabilized before use. Serial dilutions of pooled positive human sera yielded antigen-dependent limits of detection corresponding to serum dilutions of approximately 1:1700–1:5300 after a 1 h incubation at room temperature. Overnight incubation at 4 °C improved the limit of detection by at least one order of magnitude for all antigens except SCIN, with the highest sensitivity corresponding to a serum dilution of approximately 1:125,000. Clinical evaluation included serum samples from 82 patients with *S. aureus* musculoskeletal infections and 30 healthy controls. Samples were analyzed at a 1:1000 dilution after a 1 h incubation, with subsequent anti-human IgG signal amplification. Responses to IsdA, IsdB, Gmd and SCIN significantly discriminated infected patients from healthy controls. IsdB showed the highest individual discriminatory performance (AUC = 0.778), while combining IsdB, Amd, IsdA, SCIN and Hla increased the AUC to 0.861 [30].

Another multiplexing format employed glycan microarrays to distinguish influenza viruses according to their receptor-binding specificities. Amine-reactive SiO_2/Si AIR chips were functionalized with amine-PEG2-biotin, followed by avidin immobilization and stabilization of the biotin–avidin layer. Biotinylated polyacrylamide-based glycan probes were subsequently immobilized onto this layer. The array contained α2,6- and α2,3-linked sialic acid receptor analogues, together with control spots, and was blocked with D-biotin and BSA prior to analysis. Initial characterization using the α2,6-binding SNA lectin yielded a detection limit of 0.06 mg/L. The platform subsequently distinguished human pandemic H1N1pdm from avian H13N8 influenza viruses: H1N1pdm selectively bound the α2,6-linked glycan probes, whereas H13N8 preferably bound the α2,3-linked probes. Serial dilutions of H1N1pdm in 10% fetal bovine serum (FBS) yielded a detection limit of 9.29×10^8 PFU/L and a dynamic range spanning approximately three orders of magnitude [31].

Automation was introduced into AIR with the ZIVA prototype system and a 34-plex acute respiratory viral serology array designed for longitudinal antibody monitoring. Individually packaged, pre-arrayed AIR chips were housed in custom cartridges, while washing, imaging and data processing were performed automatically (Figure 4b). Each cartridge required 45 µL of sample, and a 1:20 serum dilution reduced the serum volume required to approximately 3 µL per assay. The 34-plex array included two RSV antigens, 17 influenza A and B targets, four common human coronavirus antigens, three MERS-CoV antigens, two SARS-CoV-1 antigens, and six SARS-CoV-2 antigens, covering a broad panel of respiratory viruses. Antigen-specific limits of detection were calculated independently from raw thickness measurements of four negative-control chips and defined as the mean blank thickness plus three standard deviations. Accordingly, the detection limits were reported as thickness changes rather than antibody concentrations, since converting thickness measurements into concentrations would require separate calibration curves for each antigen and was not considered appropriate for the complex human serum samples investigated. Longitudinal monitoring following SARS-CoV-2 vaccination, booster doses and breakthrough infection tracked the expected increase and subsequent decline in SARS-CoV-2 spike-specific antibody binding over time [32].

More recently, Klose et al. [33] developed a 25-plex AIR-based platform capable of simultaneously determining six cytokines and nineteen *S. aureus*-specific antibody responses. For this purpose, Si chips covered with an approximately 1400 Å-thick layer of thermally grown silicon oxide were cleaned and etched to adjust oxide thickness before being functionalized with an amine-reactive GOPTS layer. Protein antigens and cytokine-capture antibodies were deposited using a piezoelectric microarray spotter, with six replicate spots per analyte, and covalently immobilized. The surfaces were subsequently blocked with BSA/FBS and stabilized. The specific design combined direct detection of the relatively abundant anti-*S. aureus* antibody with mass-based amplification of low-abundance cytokines

using biotinylated detection antibodies and streptavidin labeled with horseradish peroxidase (HRP), and localized deposition of a precipitating HRP substrate (3,3′-diaminobenzidine, DAB). Cytokine detection limits of 13.0 ng/L for IL-6, 23.3 ng/L for IL-17A, 127.6 ng/L for IL-17F, 88.8 ng/L for IL-27, 23.5 ng/L for IL-10 and 581.1 ng/L for TNF-α, were achieved. The platform was evaluated with 429 human serum samples, including 246 from patients with culture-confirmed *S. aureus* infection and 183 controls undergoing elective surgery. After excluding samples with assay interference or incomplete data, 401 samples remained for formal analysis. IL-6 was the strongest individual predictor of infection (AUC = 0.85), whereas combining IL-6, IL-10, IL-17A, TNF-α and IsdB increased the AUC to 0.92. Thus, this detection approach enabled the simultaneous determination of low-abundance cytokines and high-abundance antigen-specific IgG to be determined in a single assay using a single sample dilution [33].

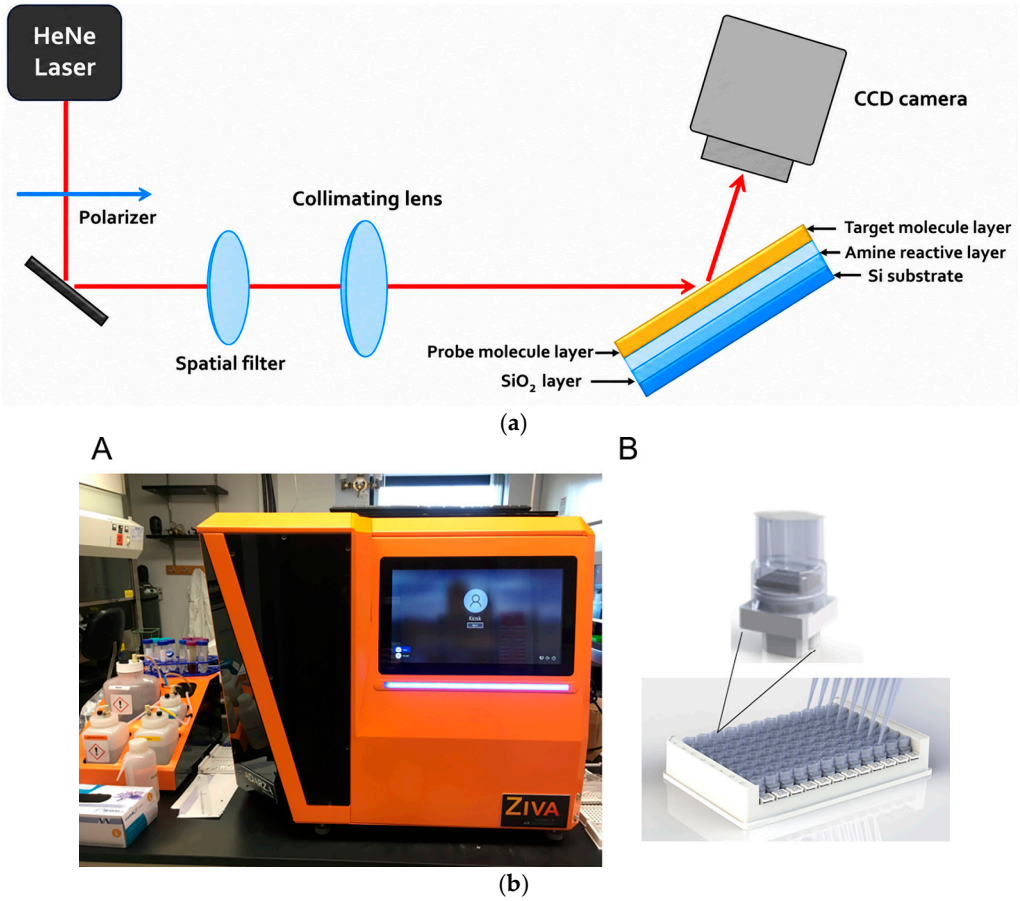

Figure 4. (**a**) Schematic of a conventional AIR setup featuring HeNe laser illumination, polarization and beam-conditioning optics, and a CCD camera for detecting the reflected light. (**b**) ZIVA system including (**A**) a fully automated instrument and (**B**) a 96-well plate filled with AIR chip cartridges and an enlarged image of a single cartridge containing an AIR chip [32].

In conclusion, AIR multiplexing has evolved along several complementary directions. Early cytokine arrays established direct parallel protein detection, while antigen microarrays extended the platform toward broad serological profiling and clinically relevant autoantibody analysis. Subsequent work increased panel size, diversified recognition chemistries and introduced automated cartridge-based operation with microliter-scale sample requirements. More recent dual-scale approaches further demonstrate that AIR can integrate direct label-free detection with selective post-binding amplification when low-abundance targets require enhanced sensitivity. The main trade-offs therefore concern assay scale, sample

complexity, incubation time, the need for amplification, and the degree of automation rather than the optical multiplexing principle itself.

2.4. Interferometric Reflectance Imaging Sensor (IRIS)

Interferometric Reflectance Imaging Sensor (IRIS) is another label-free optical sensing technology based on the interference of light reflected from a layered substrate, typically consisting of a thermally grown SiO_2 layer on a silicon substrate. Light reflected from the top surface interferes with light reflected from the Si–SiO_2 interface, generating a wavelength-dependent reflectance signal. Biomolecular binding to the functionalized sensor surface results in biomolecule accumulation, increasing the optical path difference between the top surface and the Si–SiO_2 interface and producing a measurable shift in spectral reflectivity. Analysis of these changes enables quantitative measurement of surface-bound biomolecular mass and real-time monitoring of molecular binding interactions without the need for labels [34,35].

A typical IRIS setup comprises a multi-wavelength illumination source, an imaging optical system, a SiO_2/Si sensor chip, and a CCD or CMOS camera. The sensor is sequentially illuminated at discrete wavelengths, typically using LEDs, while a low-numerical-aperture objective collects the reflected light and projects it onto the camera. Reflectance images acquired at the different illumination wavelengths are then used to reconstruct the spectral reflectivity at each location on the sensor surface (Figure 5a). Changes in optical thickness resulting from the accumulation of surface-bound biomolecules are determined by fitting the measured reflectivity data to a theoretical model based on Fresnel equations (Figure 5b). The wide-field imaging configuration also enables spatially resolved measurements across the sensor surface, allowing numerous capture spots containing different immobilized probes to be monitored simultaneously within the same field of view. This capability forms the basis for multiplexed analysis (Figure 5c) [34,35].

The multiplexing capability of IRIS has been demonstrated across a wide range of biosensing applications. One early application combined label-free whole-virus detection with multiplexed profiling of viral proteins on the same antibody-array platform. Lopez et al. [36] fabricated antibody microarrays on a Si/SiO_2 sensing surface functionalized with a copolymer coating that enabled the covalent immobilization of capture probes targeting the external glycoprotein (G), the internal matrix (M), and nucleocapsid (N) proteins of vesicular stomatitis virus (VSV). Intact VSV particles were specifically captured using antibodies targeting the external G protein, achieving a detection limit of 3.5×10^8 PFU/L. The same array was also used to distinguish multiple viral components in VSV-infected cell lysates, enabling the detection of both the external G protein and the internal M and N proteins. Furthermore, disruption of intact virions with a non-ionic surfactant enabled the simultaneous detection of the released external and internal viral proteins. Thus, IRIS enabled both whole-virus detection and multiplexed viral-protein profiling using the same antibody-array platform [36].

Highly multiplexed real-time analysis of small-molecule binding kinetics was subsequently demonstrated using the IRIS platform by Chiodi et al. (Figure 5d) [37]. The system consisted of a SiO_2/Si chip illuminated by an LED in a common-path interferometric configuration, with the reflected signal recorded by a CMOS camera. A fluidic chamber positioned over the sensing surface enabled continuous analyte delivery across microarrays of capture probes immobilized on a N,N-dimethylacrylamide-based polymer coating. An initial proof-of-concept experiment involving biotin-streptavidin binding demonstrated a mass-density detection limit of approximately 1 pg/mm^2. The optimized platform was then applied to the screening of 20 monoclonal antibodies against fumonisin B1. Each antibody was represented by 20 replicate spots, alongside 40 control spots, resulting in a total of

440 spots imaged simultaneously. A 100 µM fumonisin B1 solution was introduced over the chip for 20 min, followed by a 20 min dissociation phase using buffer. Binding was detected for 18 of the 20 antibodies. Furthermore, fitting the resulting real-time association and dissociation curves to a 1:1 Langmuir model enabled the determination of kinetic and affinity parameters for the different interactions [37].

A similar approach was subsequently employed to simultaneously evaluate the binding kinetics of multiple antibodies against anthrax lethal factor. Real-time monitoring of association and dissociation phases enabled the determination and comparison of the kinetic and affinity parameters of the different antibody–antigen interactions [38].

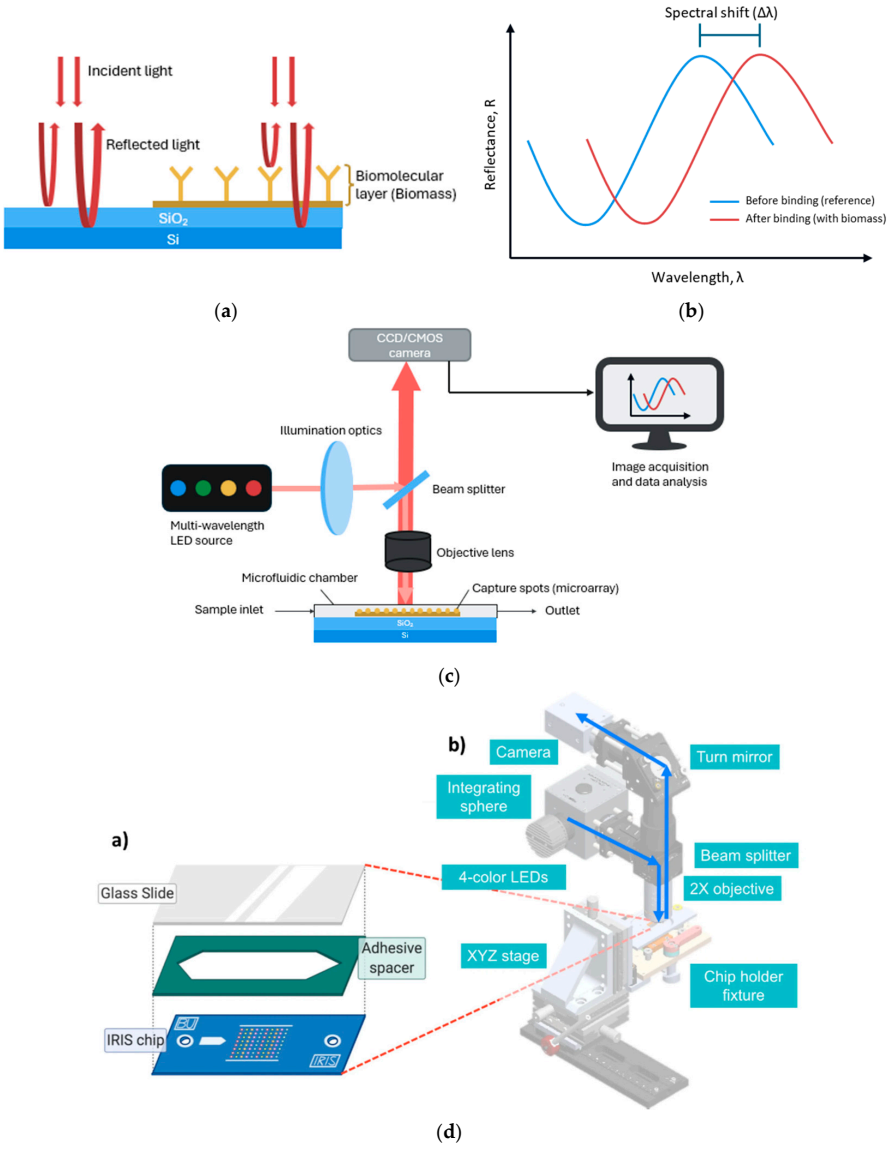

Figure 5. Schematic illustration of the operating principle and instrumentation of the f Interferometric Reflectance Imaging Sensor (IRIS). (**a**) Light interference at the Si/SiO_2 sensor interface before and after biomolecular binding. (**b**) Binding-induced shift in the spectral reflectance profile. (**c**) Typical multi-wavelength IRIS setup, comprising LED illumination, beam-splitting optics, a microfluidic system, and CCD/CMOS imaging. (**d**) Schematic illustration of the fluidic cartridge and the IRIS setup for monitoring of multiplexed biomolecular interactions: a) the red dashed lines indicate the location of the fixture that secures the cartridge/chip inside the setup, while b) the blue arrows show the light path in the interferometer [37].

A significant advancement of the IRIS platform is Single-Particle IRIS (SP-IRIS), which extends conventional IRIS from the detection of accumulated surface-bound biomolecules to the detection and characterization of individual biological nanoparticles. In SP-IRIS, the layered SiO_2/Si sensor structure interferometrically enhances the optical scattering signal from individual captured particles, providing sufficient optical contrast for their direct visualization and digital counting [39,40]. SP-IRIS has been used to detect individual exosomes in a label-free, multiplexed format. Antibody microarrays containing capture probes against the exosomal tetraspanins CD9, CD63 and CD81 enabled the selective capture of different exosome subpopulations at spatially distinct sensing spots. Following capture, individual exosomes were directly visualized and digitally counted. The interferometric signal also enabled particle-size discrimination, with particles larger than approximately 50 nm being detectable. Detection limits of 5.07×10^{12} particles/L and 3.94×10^{12} particles/L were achieved using CD63 and CD81 capture antibodies, respectively [39].

For multiplexed virus detection, Seymour et al. [40] further developed SP-IRIS by introducing a DNA-directed antibody immobilization strategy. Three distinct single-stranded DNA (ssDNA) probes were patterned on the sensor chip and subsequently converted into a multiplexed antibody array through sequence-specific hybridization with DNA-conjugated antibodies targeting the surface glycoproteins of Ebola, Marburg and Lassa viruses. Using this configuration, three recombinant vesicular stomatitis virus (rVSV) models expressing the corresponding viral glycoproteins were specifically detected in real time, with no detectable cross-reactivity between the three capture regions. The study also introduced a homogeneous assay format in which the virus-containing sample was first mixed with the antibody–DNA conjugate and subsequently applied to the sensor, where the complexes were captured by complementary DNA spots. This approach eliminated the need for separate antibody spotting to establish spatially distinct capture regions. Using rVSV-EBOV as a model, a concentration of 100,000 PFU/L was detected after 1 h of incubation, with an estimated detection limit of 43,000 PFU/L. Furthermore, integration of the homogeneous assay into a passive microfluidic cartridge further reduced the analysis time, enabling the detection of 10^7 PFU/L rVSV-EBOV in approximately 6 min [40].

Beyond pathogen detection, SP-IRIS has also been applied to the phenotyping of individual extracellular vesicles (EV) in neurological disease using clinically derived biofluids. Bravo-Miana et al. [41] used the SP-IRIS-based ExoView R200+ platform to analyze paired cerebrospinal fluid (CSF) and serum samples from 10 patients with relapsing-remitting multiple sclerosis (RRMS), nine with primary progressive multiple sclerosis (PPMS), and 10 non-MS controls, without prior EV isolation. Tetraspanin chips targeting CD63, CD81 and CD9, together with customized capture regions for L1CAM and GLAST, were used to characterize putative neural EV populations at the single-particle level [41].

More recently, SP-IRIS was adapted for the direct analysis of EVs secreted by human adipose tissue (adipo-chip). The platform incorporated capture antibodies targeting the conventional EV tetraspanins CD9, CD63 and CD81 together with antibodies against the adipose-associated markers CAVN-1 and PLIN1. Lago-Baameiro et al. [42] evaluated the platform using 26 secretome samples obtained from visceral and subcutaneous adipose tissue explants from 13 individuals with severe obesity undergoing bariatric surgery. EVs were captured directly from the secretomes without prior purification, while interferometric detection enabled their enumeration and size characterization. Further phenotypic characterization was achieved using four fluorescently labelled detection antibodies targeting TGFBI, mimecan, FABP4 and ceruloplasmin, thereby enabling multiplexed analysis of EV biomarkers associated with obesity and adiposity [42].

To further adapt IRIS technology for point-of-care virus detection, Pixel-Diversity IRIS (PD-IRIS) was introduced as an extension of SP-IRIS that replaces conventional z-scan

acquisition with multispectral detection from a single image. Aslan et al. [43] applied PD-IRIS to the label-free detection of intact Monkeypox virus (MPXV), using an anti-A29 monoclonal antibody for virus recognition and Protein G spots on the sensor surface for antibody capture. The system achieved a calculated detection limit of approximately 200,000 PFU/L (~3.3 aM), compared with a detection limit of 1,800,000 PFU/L for the corresponding ELISA. Specificity was also demonstrated against HSV-1 and cowpox virus. Real-time measurements produced a significant signal in less than 10 min for MPXV concentrations of 5×10^7 and 1×10^7 PFU/L, while the complete sample-to-result workflow was estimated to take approximately 20 min. By eliminating the mechanically and computationally demanding z-scan required in conventional SP-IRIS, PD-IRIS offers a more compact and rapid configuration, with potential applications in point-of-care pathogen detection [43].

Another advancement of the conventional IRIS platform is multi-parametric IRIS (MP-IRIS), which has been developed to dynamically compensate for bulk refractive-index effects during real-time binding measurements through dual-wavelength detection. This configuration supports label-free, multiplexed binding kinetic measurements while reducing the contribution of bulk refractive-index changes to approximately 3 pg/mm^2 for a refractive-index variation of 10^{-3} RIU. Aslan et al. [44] validated its performance through multiplexed DNA hybridization assays. Under changes in background optical thickness that introduced measurement errors of up to approximately 60% with single-wavelength detection, the dual-wavelength approach maintained quantification variations below 10%, demonstrating substantially improved measurement repeatability [44].

Collectively, these developments demonstrate that IRIS multiplexing has evolved along several complementary directions rather than simply through an increase in the number of simultaneously detected targets. Conventional IRIS enables dense microarray-based screening of binding kinetics and simultaneous molecular profiling, whereas SP-IRIS extends these capabilities to the digital counting and size-resolved characterization of individual nanoparticles. DNA-directed capture strategies and passive microfluidic integration further enhance assay configurability and reduce analysis times, particularly for viral detection. Meanwhile, clinical EV studies demonstrate the potential of SP-IRIS for analyzing complex biological samples, although these applications may combine interferometric particle counting with fluorescence-based phenotypic characterization. Finally, PD-IRIS and MP-IRIS address important practical limitations related to acquisition complexity and measurement robustness, respectively. These developments highlight the versatility of IRIS-based multiplexing and the different trade-offs involved in its implementation, depending on whether the primary objective is the determination of binding kinetics, single-particle resolution, compatibility with clinical samples, assay simplicity, or robustness under variable measurement conditions.

2.5. Mach–Zehnder Interferometers (MZIs)

Mach–Zehnder interferometers (MZIs) are optical waveguide sensors that combine evanescent-field sensing with optical phase-difference measurements. In a conventional MZI configuration, the input light is split into two optical paths: a sensing arm and a reference arm, which are subsequently recombined at the output (Figure 6a). The sensing arm interacts with the sample through the evanescent field of the guided optical mode, whereas the reference arm is either isolated from the environment or exposed to a reference medium. Biomolecular binding at the functionalized surface of the sensing arm alters the local refractive index within the evanescent field, thereby changing the effective refractive index and propagation phase of the guided mode. This produces a phase difference between the light propagating through the sensing and reference arms. Upon recombination, the

phase difference is converted into a measurable change in output intensity, enabling real-time, label-free monitoring of biomolecular reactions [5,45].

A conventional integrated MZI biosensing system typically consists of a monochromatic light source, an input coupling element (e.g., a grating coupler), a waveguide structure containing sensing and reference arms, an optical recombination region and a photodetector. In practical biosensing implementations, a flow cell can be integrated above the sensing region to enable the controlled delivery of samples and reagents, facilitating real-time measurements under defined experimental conditions [5,45].

Broad-band Mach–Zehnder interferometry (BB-MZI) extends the conventional MZI concept by replacing monochromatic excitation with broad-band illumination and monitoring the full transmission spectrum of the interferometer. In the integrated BB-MZI platform (Figure 6b), arrays of ten planar silicon nitride interferometers are monolithically integrated on a silicon chip, together with their individual broad-band silicon avalanche light-emitting diodes [45–47]. The modulated output spectra are collected from the chip edge via an external optical fiber and directed to a miniaturized spectrometer, while dedicated control electronics enable sequential interrogation of the ten interferometers. A microfluidic module positioned over the exposed sensing regions ensures continuous delivery of samples and reagents. Biomolecular interactions alter the effective refractive index of the sensing arm, resulting in wavelength-dependent shifts in the output spectrum. Fourier-domain processing converts these spectral changes into phase shifts, enabling real-time monitoring of binding events and independent analysis of the TE and TM polarization responses [45–47]. The integration of multiple MZIs on a single photonic chip enables compact sensor architectures and the sequential interrogation of multiple sensing regions.

An early implementation of multiplexed BB-MZI sensing employed a silicon chip containing ten independently addressable interferometers for the simultaneous detection of streptavidin and anti-mouse IgG antibodies. Following oxygen-plasma cleaning and hydrophilization, the sensing surfaces were modified with APTES and spotted with mouse IgG, biotinylated BSA or BSA as a blank control, followed by BSA blocking. The ten sensing arms were divided into groups functionalized with the different recognition molecules. Analyte solutions were delivered through an integrated fluidic cell, while the interferometers were sequentially interrogated using LED multiplexing. The analyte mixtures contained streptavidin at concentrations ranging from 2 pM to 2.5 nM and anti-mouse IgG antibodies from 25 pM to 66.7 nM. Streptavidin was detected at concentrations as low as 5 pM. For anti-mouse IgG, detection limits of 32 pM and 40 pM were obtained using TE- and TM-phase analysis, respectively, with a linear response extending to 3.3 nM [46].

Food allergen analysis provided another demonstration of BB-MZI multiplexing, enabling the simultaneous determination of bovine κ-casein, peanut protein, soy protein, and gliadin [47]. A specially designed, nearly one-dimensional microfluidic module ensured uniform reagent delivery across the ten interferometers. The chips were hydrophilized by oxygen-plasma treatment, functionalized with APTES and spotted with the four allergen proteins. The ten BB-MZIs were arranged as four allergen-specific pairs, while two BSA-coated interferometers served as controls for nonspecific binding. The competitive immunoassay included a 10 min preincubation of calibrators or samples with a mixture of allergen-specific antibodies, followed by signal enhancement using secondary anti-species antibodies. All four allergens were determined within 6.5 min, with detection limits of 0.04, 1.0, 0.80 and 0.10 mg/L for κ-casein, peanut protein, soy protein and gliadin, respectively. The corresponding linear ranges were 0.10–2.0, 2.0–20, 2.0–16 and 0.20–20 mg/L. Recovery values ranged from 87.5 to 110%, while intra-assay CVs ranged from 4 to 8% and inter-assay CVs from 12 to 16%, respectively. The system was also evaluated with rinsing-water samples from the cleaning-in-place system of a dairy facility. A total of 23 spiked samples were

analyzed and compared with the corresponding in-house ELISA results, showing good agreement between the two methods [47].

BB-MZI multiplexing was subsequently extended to mycotoxin analysis through the simultaneous determination of aflatoxin B1 (AFB1), fumonisin B1 (FB1) and deoxynivalenol (DON) in beer [48]. Following O_2-plasma hydrophilization and APTES functionalization, the chips were spotted with AFB1-BSA, FB1-OVA or DON-OVA conjugates, while one interferometer coated with OVA served as a blank control. The competitive two-step immunoassay involved mixing calibrators or diluted beer samples with monoclonal antibodies against the three mycotoxins and passing the mixtures over the chip for 8 min, followed by a 4 min reaction with a secondary anti-mouse IgG antibody. All three analytes were determined within 12 min, with detection limits of 0.8, 5.6 and 20 µg/L for AFB1, FB1 and DON, respectively, in undiluted beer. Fortified beer samples yielded recovery values from 85 to 115%. Furthermore, the analysis of 29 beers of different types and origins showed overall good agreement with ELISA results and, for selected samples, with LC-MS/MS measurements. The chip could also be regenerated and reused for at least 20 assay cycles [48].

BB-MZI arrays have also been applied to simultaneous detection of *Salmonella typhimurium* and *Escherichia coli O157:H7* in drinking water and milk (Figure 6b) [49]. Three MZIs were coated with *S. typhimurium* lipopolysaccharide (LPS), four with *E. coli* LPS, and the remaining three with BSA to monitor nonspecific binding. The competitive three-step immunoassay involved reaction of the sample with bacteria-specific antibodies, followed by the addition of biotinylated anti-species-specific secondary antibodies and streptavidin for signal enhancement. Analytical sensitivity was improved by heating bacterial samples at 90 °C for 10 min, followed by ultrasonication for 5 min. Detection limits of 40,000 CFU/L for *S. typhimurium* and 110,000 CFU/L for *E. coli O157:H7* were achieved, with dynamic ranges of 2×10^5–10^9 and 3×10^5–10^9 CFU/L, respectively. The assay required 10 min for drinking water samples and 15 min for milk samples, for which additional washing steps were introduced to minimize matrix effects. Recovery values in spiked bottled-water and milk samples ranged from 90 to 112%, while intra- and inter-assay CVs were below 5% and 7%, respectively. Detection at the level of a single bacterium in 25 mL of sample required an additional pre-enrichment step of 7.5 h [49].

More recently, an all-in-one monolithic photonic chip further advanced BB-MZI multiplexing towards on-site food-contaminant analysis [50]. The 37-mm^2 chip integrated ten BB-MZIs with their individual broad-band silicon light sources, as well as on-chip spectral analyzers based on arrayed waveguide gratings and photodiode arrays, thereby eliminating the need for an external spectrometer. The chip operated in a portable automated reader incorporating fluidic and electrical interfaces, a peristaltic micropump, control electronics, and software for real-time signal monitoring. For allergen detection, BB-MZI pairs were functionalized with bovine κ-casein, peanut protein, or gliadin, while BSA-coated interferometers served as controls for nonspecific binding. Separate BB-MZI pairs carrying FB1-OVA and DON-OVA conjugates were used for mycotoxin analysis, with OVA-coated sensors serving as controls. Both applications relied on competitive immunoassays incorporating secondary-antibody signal enhancement. The three allergens were simultaneously determined in dairy-industry rinsing water in 10 min, with detection limits of 0.01, 0.25 and 0.05 mg/L for κ-casein, peanut protein and gliadin, respectively. FB1 and DON were simultaneously determined in beer within 15 min, with detection limits of 2.0 and 10 µg/L, respectively. Allergen recovery values ranged from 87.5 to 112%. Overall, the fully integrated architecture enabled real-time multiplexed measurements in a compact portable format [50].

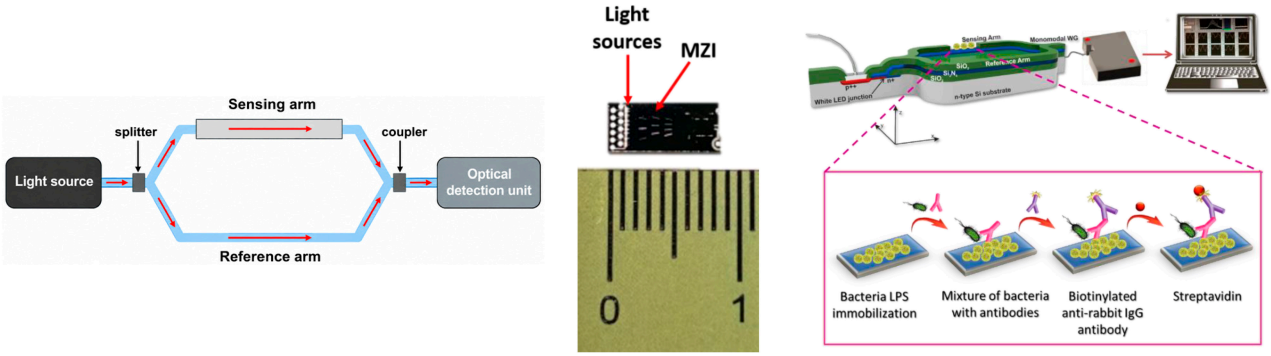

(**a**) (**b**)

Figure 6. (**a**) Schematic illustration of a conventional Mach–Zehnder interferometer (MZI) biosensor. The input light is split into sensing and reference arms. Binding events in the sensing arm induce a phase shift, which is detected upon recombination of the two optical signals. (**b**) (**left**) Photograph showing the actual dimensions of a chip accommodating 10 integrated silicon-nitride waveguide MZIs along with their corresponding broad-band white light silicon LEDs; (**right**) 3D schematic of the competitive assay configuration for bacterial detection using the integrated silicon-nitride waveguide MZI sensor [49]. The bacteria in the sample competed with the immobilized on the sensor respective LPS for binding to the bacteria-specific antibody. Biotinylated secondary antibody and streptavidin were subsequently used for signal enhancement.

An MZI-based point-of-care system was also developed for multiplexed miRNA detection in human urine, employing an integrated silicon nitride slot-waveguide architecture [51]. The chip incorporated four MZI sensors, each comprising a strip-waveguide reference arm and a 7 mm slot-waveguide sensing arm, while vertical grating couplers provided optical input and output. An infrared InGaAs camera simultaneously monitored the output intensity of the individual interferometers, enabling real-time tracking of phase changes associated with DNA–miRNA hybridization. For multiplex analysis, different complementary DNA capture probes were covalently immobilized by microarray spotting onto the amine-modified sensing surfaces of individual MZIs. Synthetic miR-21 and let-7a were detected over a concentration range of 1 nmol/L to 1 µmol/L, with a lowest detectable concentration of 1 nmol/L for both targets and an assay time of 15 min. The platform was subsequently applied to the simultaneous, label-free and amplification-free detection of miR-21 and let-7a in urine samples from three patients with late-stage bladder cancer and two healthy controls. Both targets were determined in a single 15 min reaction [51].

A different MZI architecture is the asymmetric Mach–Zehnder interferometer (aMZI), in which a small optical path-length difference is introduced between the two interferometer arms. This asymmetry makes the phase difference wavelength-dependent, producing a periodic transmission spectrum that can be followed during wavelength scanning. Refractive-index changes at the sensing arm modify its effective optical path length, resulting in a shift in the interference pattern. The analytical sensitivity can be tuned by adjusting the geometrical path length of the sensing region and the degree of asymmetry between the two arms, supporting highly sensitive refractive-index measurements [52]. Multiplexed aMZI biosensing was demonstrated through the simultaneous detection of anti-SARS-CoV-2 antibodies in human plasma [52]. The photonic chip incorporated six sensing aMZIs and two auxiliary interferometers, with input light distributed through an on-chip 1 × 8 splitter. The Si_3N_4 sensing regions were selectively modified with a carboxylate-terminated coating, while the surrounding SiO_2 surface was functionalized with a PEG-based antifouling layer. Following EDC/NHS activation, spike protein (SP), receptor-binding domain (RBD), and nucleocapsid protein (NP) were immobilized on different sensing regions, together with BSA control spots, thereby enabling multiplexed antibody detection on a single chip.

Anti-SARS-CoV-2 antibodies were initially detected directly through their binding to the immobilized viral antigens. Analytical sensitivity was subsequently enhanced by incubation with a secondary anti-human IgG antibody. Direct detection yielded detection limits of 1.4, 9.7 and 4.8 IU/mL for anti-SP, anti-RBD and anti-NP antibodies, respectively, while the indirect assay reduced them to 0.3, 0.5 and 2.0 IU/mL. The platform was evaluated using a National Institute for Biological Standards and Control (NIBSC) verification panel comprising 23 antibody-positive and 14 antibody-negative plasma samples. Comparison with several serological methods showed overall good agreement [52].

Overall, the evolution of MZI biosensing is characterized not simply by an increase in the number of simultaneously detectable targets, but by the progressive integration of multiplexing with photonic integration, rapid assay formats, and analysis of complex biological and food matrices. Early BB-MZI arrays established the feasibility of multianalyte detection using multiple functionalized interferometers, although they relied on external spectral readout. Subsequent food-analysis applications extended this architecture to the detection of proteins, small molecules, and bacteria. The development of the all-in-one BB-MZI platform further reduced the instrumentation requirements by integrating spectral analysis and photodetection on-chip, while the miRNA and aMZI studies demonstrated multiplexed analysis directly in human urine and plasma, respectively. Across these implementations, label-free optical transduction remains a common feature of MZI biosensing, although the associated assay workflows vary considerably. Nucleic-acid detection can be performed without amplification or labeling, whereas several immunochemical applications employ secondary antibodies or streptavidin to enhance analytical sensitivity.

2.6. Bimodal Interferometers (BiMW)

Bimodal waveguide interferometers (BiMW) offer an alternative to conventional Mach-Zehnder Interferometers (MZIs) for biosensing applications. They employ a single-channel waveguide structure that supports two orthogonal modes of the same polarization, enabling the detection of differential phase shifts induced by light-matter interactions at the sample interface (Figure 7a) [53,54]. Although achieving optimal detection performance requires precise and non-trivial alignment of an off-axis single-mode input to ensure equal excitation of both modes, the single-channel architecture reduces the physical footprint by approximately half compared to conventional MZIs. Recent advances have further improved BiMW performance through the incorporation of periodic structures operating in subwavelength grating or photonic crystal regimes [54]. These configurations introduce distinctive dispersive properties and enhance light-matter interactions, thereby significantly increasing sensing sensitivity and offering considerable potential for integration into multi-biosensor chips. BiMW biosensors have been employed in a broad range of biomedical and environmental applications [54]. Most reported applications, however, have focused on the detection of a single analyte.

The challenge of achieving multiplexed detection was addressed through the development of a nanophotonic interferometric biosensor that combines a CMOS-fabricated BiMW chip with a custom-designed polymer microfluidic delivery system (Figure 7b) [55]. The chip incorporates an on-chip beam splitter that distributes light from a single source across eight parallel waveguide channels. Signal readout is performed using a dedicated silicon photodetector array and a miniaturized amplifier, enabling simultaneous data acquisition across all channels. This cost-effective, laser-diode-driven prototype maintains the high performance of its single-waveguide predecessor, with a bulk refractive index limit of detection of 2–5 × 10^7 RIU. Its biosensing capabilities have been validated through the detection of Respiratory Syncytial Virus (RSV) nucleoproteins. Specifically, RSV B nucleoprotein was detected in less than 9 min, with a detection limit of 1.2 (±0.4) µg/L across the seven sensors.

Nevertheless, fully exploiting the multiplexing capabilities of this biosensing architecture requires further development of selective and controlled biofunctionalization of individual waveguides. Such functionalization would enable the simultaneous detection of different target analytes on a single photonic chip, thereby achieving true multiplexed biosensing.

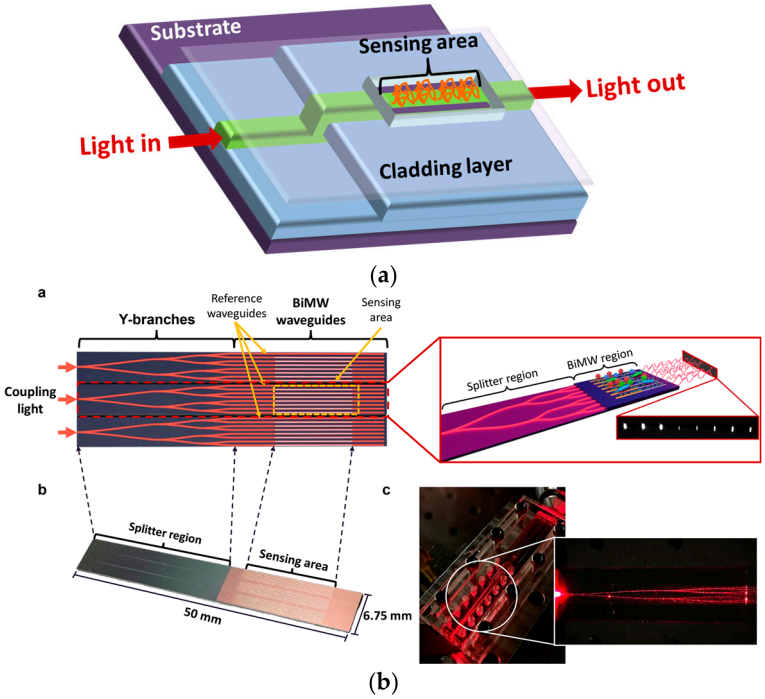

Figure 7. (**a**) Schematic illustration of a Bimodal waveguide interferometer. (**b**) Schematic layout of the multiplexed photonic chip. Each chip integrates three multiplexed sensors (a); one sensor is highlighted, showing a rendered image of the multiplexed BiMW nanophotonic sensor chip (b). A picture showing the eight output light spots captured on a CCD camera is also included (c), together with a photograph of the multiplexed BiMW nanophotonic sensor chip, as well as photographs of the sensor chip placed in the experimental setup and the simultaneous light coupling to eight waveguides [55].

2.7. Surface Plasmon Resonance and Surface Plasmon Resonance Imaging (SPR/SPRi)

Surface Plasmon Resonance (SPR) is based on surface plasmons, which are electromagnetic waves associated with the collective oscillations of free conduction electrons at a metal-dielectric interface [56,57]. Resonance occurs when the evanescent field generated by p-polarized light under conditions of total internal reflection couples with surface plasmons, resulting in a characteristic minimum in reflected-light intensity at a specific angle of incidence or wavelength [57,58]. The binding of biomolecules to the sensor surface alters the local refractive index, thereby shifting the resonance condition [57,59]. Monitoring this shift in real-time enables the label-free detection of biomolecular interactions and provides information on analyte concentration, binding affinity, and association and dissociation kinetics [56–58].

A typical SPR biosensor consists of a light source, a coupling element, a metal-coated sensing surface, a flow system for sample delivery, and a photodetector. Among the different excitation configurations, prism coupling based on the Kretschmann configuration is the most widely used (Figure 8a). In this arrangement, p-polarized light passes through a high-refractive-index prism and reaches a thin metal film, typically made of gold because of its chemical stability. The reflected light is then collected by a detector. The SPR response is monitored by measuring changes in the resonance angle or wavelength. Sensor performance depends on several parameters, including the angle of incidence, excitation wavelength,

refractive indices of the prism and surrounding medium, and the properties of the metal film. Although prism-coupled SPR systems are well established, their optical requirements often result in relatively bulky instrumentation. Consequently, more recent developments have focused on simplifying the optical path and coupling geometry to facilitate the development of compact, portable and multichannel SPR platforms [56,59].

Surface Plasmon Resonance imaging (SPRi) extends conventional SPR by enabling spatially resolved and higher-throughput analysis. Rather than monitoring a single sensing region, SPRi employs an area detector, typically a CCD or CMOS camera, to record reflected-light intensity across a two-dimensional sensing surface. In a typical prism-coupled SPRi system, measurements are performed at a fixed angle of incidence, and local refractive-index changes resulting from molecular binding are detected as spatial variations in reflected light intensity. The ability to resolve these changes at different positions on the sensor surface enables the parallel monitoring of multiple molecular interactions and facilitates microarray-based multiplexed analysis. However, this increase in throughput may be accompanied by lower sensitivity than that of conventional SPR, particularly in intensity-based SPRi measurements [60–62].

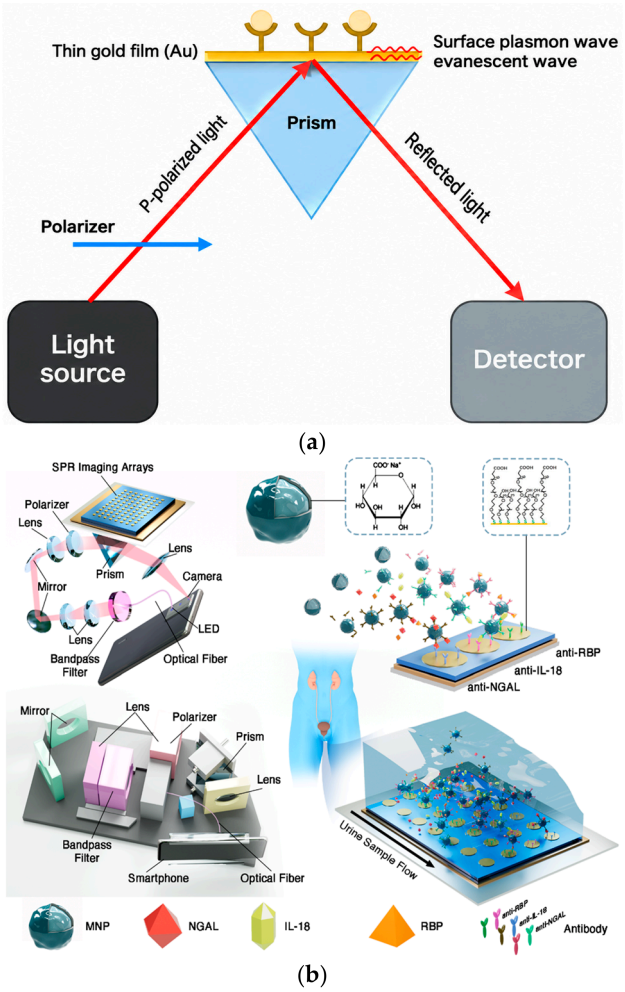

Figure 8. (**a**) Schematic illustration of a prism-coupled SPR biosensor in the Kretschmann configuration. P-polarized light excites surface plasmons at the gold film, while biomolecular binding alters the local refractive index, resulting in a shift in the resonance condition. (**b**) Principle of the smartphone SPRi system for the detection of biomarkers related to acute kidney injury (NGAL, IL-18 and RBP) in urine by sandwich immunoassays [63].

Zhang et al. [63] developed a smartphone-based SPRi system for the simultaneous determination of three acute kidney injury biomarkers, namely NGAL, IL-18, and RBP, in urine (Figure 8b). The platform incorporated a 12-spot gold array arranged in four rows, with three functionalized with capture antibodies against NGAL, IL-18, and RBP, respectively, and the fourth with BSA as a control. The gold surface was modified with a mixed thiol-PEG/thiol-COOH self-assembled monolayer, followed by EDC/NHS activation to enable covalent antibody immobilization. Hydrophilic gold spots were patterned on a hydrophobic glass background to facilitate selective functionalization and minimize cross-contamination between spots. The smartphone LED flash served as the excitation source, while its camera recorded the reflected light signal. Signal enhancement was achieved using a sandwich immunoassay incorporating antibody-functionalized magnetic nanoparticles. Calibration in urine yielded detection limits of 0.19 μg/L for NGAL, 0.51 μg/L for IL-18 and 0.70 μg/L for RBP. Analysis of urine samples spiked with known concentrations of all three biomarkers resulted in an average recovery of 99.86 ± 5.12%. Finally, the platform was evaluated using real urine samples from two patients with acute kidney injury and one healthy volunteer, demonstrating the simultaneous determination of NGAL, IL-18 and RBP [63].

Cancer biomarker detection has also been investigated using a gold-based SPRi biochip for simultaneous determination of CA-125 and mesothelin [64]. The gold surface was modified with a 11-mercaptoundecanoic acid self-assembled monolayer, followed by EDC/NHS activation to facilitate the covalent immobilization of the bioreceptors. Spatially separated spots containing anti-CA-125 and anti-mesothelin antibodies were generated on the same biochip, together with anti-IgG and anti-BSA spots serving as negative controls. Antibody-functionalized gold nanoparticles were subsequently introduced for selective target capture and signal enhancement. Individual biomarker detection in solution yielded detection limits of 13.62 nM for CA-125 and 3.03 nM for mesothelin. Simultaneous measurements in fetal bovine serum containing both biomarkers at a concentration of 9 nM resulted in reflectivity changes of 1.7 ± 0.1% and 3.2 ± 0.2% at the anti-CA-125 and anti-mesothelin spots, respectively. In comparison, the corresponding negative-control spots exhibited changes of 0.02 ± 0.01% and 0.48 ± 0.02%. However, the system was not evaluated with clinical patient samples [64].

Ucak-Ozkaya et al. [65] developed a magnetic-bead-assisted SPRi array for the detection of four prostate cancer-associated biomarkers: PSA, IGF-I, VEGF-D, and CD14. The system incorporated a 16-spot gold SPR chip functionalized with primary antibodies against the selected biomarkers, with BSA included as a negative control. The chip was integrated into a 3D-printed microfluidic channel. Target antigens were initially captured offline using magnetic beads functionalized with secondary antibodies and subsequently introduced over the SPRi chip, where their interactions with the corresponding immobilized capture antibodies were monitored in real time. Detection limits of 7.6 ng/L for CD14, 5.8 ng/L for IGF-I and 5.3 ng/L for VEGF-D were achieved, with corresponding dynamic ranges of 1–100, 1.1–110 and 0.5–100 ng/L, respectively. PSA was evaluated separately during assay optimization, yielding a dynamic range of 0.625–100 ng/L and a detection limit of 0.625 ng/L. Although clinical samples were not included, the study demonstrated the potential of magnetic-bead-assisted SPRi for highly sensitive, multiplexed detection of prostate cancer-associated biomarkers [65].

SPRi has also been applied to multiplexed food-safety analysis. Miyake et al. [66] developed a six-plex SPR imaging immunosensor for the simultaneous determination of azoxystrobin, boscalid, chlorfenapyr, imazalil, isoxathion and nitenpyram in crop samples. The system combined SPR imaging with a microarray-type sensor chip consisting of a gold-coated glass prism modified with a carboxylated alkanethiol layer containing NHS-activated

groups. Hapten–BSA conjugates corresponding to the six pesticides were immobilized at distinct locations on the chip, followed by deactivation with ethanolamine and blocking with BSA. Detection was based on a competitive inhibition format, i.e., pesticide-containing samples were mixed with the corresponding monoclonal antibodies before injection over the array. Consequently, increasing pesticide concentration reduced antibody binding to the immobilized hapten-BSA conjugates. The multiplexed assay exhibited working ranges of 3.5–19 μg/L for azoxystrobin, 4.5–50 μg/mL for boscalid, 2.5–25 μg/L for chlorfenapyr, 5.5–50 μg/mL for imazalil, 3.5–50 μg/L for isoxathion and 8.5–110 μg/L for nitenpyram. Analysis of tomato samples spiked with all six pesticides yielded recoveries of 90–119%, with relative standard deviation (RSD) values of 0.8–8.5%. Comparison with chromatographic reference methods was performed using vegetable samples cultivated with azoxystrobin, boscalid and nitenpyram; vegetable samples spiked with chlorfenapyr and isoxathion; and commercial lemon samples containing imazalil. Good agreement between the SPRi sensor and the corresponding HPLC or LC-MS/MS methods was obtained for five of the six pesticides, with R^2 values ranging from 0.91 to 0.99. Nitenpyram remained the main limitation, as the sensitivity of the SPR system was insufficient for its reliable determination in incurred samples [66].

Stojanović et al. [67] extended the array format to a 44-plex antibody panel for the simultaneous, label-free analysis of cell-surface antigens on viable cancer cells using an SPRi platform. The sensors were pre-activated and coated with a 100 nm-thick hydrogel-like layer, which was subsequently patterned using a continuous-flow microfluidic spotter to produce 44 antibody-functionalized spots targeting cell-surface receptors, together with four negative-control spots. The resulting 6 × 8 array covered an imaging area of 6 × 8 mm, with individual antibody spots measuring 500 × 830 μm^2. Cell suspensions at a concentration of 1×10^9 cells/L were introduced onto the sensor surface and allowed to sediment and interact with the immobilized antibodies for 15 min, enabling the simultaneous profiling of cell-surface antigen expression. Five cancer cell lines were investigated, and the SPRi responses were compared with quantitative flow cytometry measurements. For positively expressed markers, the overall correlation between the two methods was $R^2 = 0.76$, with individual-cell-line correlation coefficients ranging from 0.67 to 0.91. The SPRi measurement itself required less than 20 min, whereas sensor preparation and sensorgram acquisition required approximately 1 h and 45 min, respectively. The study was designed as a proof-of-concept demonstration of semi-quantitative cell-surface profiling rather than clinical biomarker quantification. Nevertheless, it highlighted the potential of SPRi arrays for rapid, high-content profiling of cell-surface antigen expression [67].

Multiplexed clinical profiling of circulating extracellular vesicles (EVs) was demonstrated by Shibuta et al. [68] using SPRi to identify disease- associated surface-marker signatures in patients with type 2 diabetes mellitus (T2DM) and hypertension (HT). Serum-derived EVs were isolated by polyethylene glycol precipitation and analyzed with an SPRi system equipped with a gold biochip bearing duplicate antibody- and lectin-functionalized spots. The study included 71 patients with T2DM, 47 patients with HT and 18 healthy controls. Each specimen could be analyzed in approximately 15 min, highlighting the potential of SPRi for rapid, multiplexed EV phenotyping in clinical samples [68].

Multiplexed SPRi analysis of circulating EVs has also been investigated for the identification of potential biomarkers of tissue damage and recovery following ischemic stroke. Picciolini et al. [69] analyzed serum-derived small EVs from 19 patients with subacute ischemic stroke and 20 age- and sex-matched healthy controls using a gold SPRi biochip bearing 12 ligand families, including positive and negative controls, which enabled the simultaneous detection of 10 EV subpopulations. The capture ligands targeted EVs of

endothelial, neuronal, microglial and astrocytic origin, as well as markers associated with aging and apoptosis [69].

Overall, SPRi-based multiplexing encompasses a broad range of assay configurations, extending from low-plex biomarker panels to high-density cellular and extracellular vesicle profiling. The main differences among these approaches lie less in the optical readout itself than in the assay architectures employed to achieve the required sensitivity and biological specificity. Smartphone-based and cancer biomarker detection platforms have combined SPRi with magnetic nanoparticles, gold nanoparticles, or magnetic-bead-assisted pre-capture to enhance analytical performance. In contrast, pesticide analysis and high-density cell-surface profiling demonstrate that multiplexed measurements can also be achieved through direct or competitive SPR readout without relying on additional signal-amplification strategies. The achievable degree of multiplexing is therefore highly application-dependent, ranging from two or three soluble biomarkers to six pesticides, 44 cell-surface markers, and multiple EV subpopulations. The level of clinical validation also varies considerably. While some studies remain proof-of-concept demonstrations based on model or spiked samples, more recent applications involving EVs have been evaluated in defined patient cohorts and provide phenotypic information extending beyond simple analyte quantification. Thus, SPRi offers considerable flexibility for spatial multiplexing, although this versatility involves trade-offs among multiplexing capacity, assay complexity, reliance on secondary signal amplification or pre-capture steps, portability, and the extent of clinical validation.

3. Comparative Assessment of Label-Free Optical Biosensing Platforms

Across the platforms reviewed, high analytical sensitivity has been demonstrated for a broad range of target classes. However, direct comparisons of reported detection limits remain challenging because of differences in analyte type, assay format, sample matrix, amplification strategy and performance metrics. AIR platforms have achieved ng/L-level detection for several soluble biomarkers, while increasingly combining analytical sensitivity with diagnostic discrimination in multiplex serological and cytokine panels. Similarly, MZI-based sensors have demonstrated broad analytical performance covering applications from protein biomarkers and nucleic acid detection to whole-bacterium analysis. WLRS platforms have also achieved low detection limits across clinical, food, microbial and environmental applications. For IRIS and SPRi, analytical sensitivity is often complemented with imaging-derived information, such as digital single-particle detection, phenotypic profiling, and spatially resolved multiplexing. Consequently, their overall analytical performance cannot always be adequately captured by a single limit-of-detection value. RIfS performance, in turn, is more strongly dependent on sensor architecture, with reported metrics including spectral shifts, changes in effective optical thickness, concentration thresholds, kinetic parameters, diagnostic sensitivity and specificity. Therefore, analytical sensitivity should be interpreted in the context of both the type of information generated and the experimental conditions under which it is measured. To enable a more direct comparison of representative multiplexed implementations, Table 1 summarizes the key practical and analytical characteristics of the reviewed platforms, including multiplexing strategy, number of targets, assay time, sample requirements, validation level, instrumentation, portability, and use of signal amplification.

Table 1. Comparative overview of representative multiplexed label-free optical biosensing implementations, highlighting multiplexing strategy, number of simultaneously detected targets or interactions, assay time, sample requirements and validation, detection mode and instrumentation, portability, and label or amplification status.

Platform [Ref.]	Multiplexing Format	Number of Targets	Assay Time	Sample/Validation	Detection Mode/Portability	Direct Detection/ Signal Amplification
pi-RIfS [14]	antiphospholipid-syndrome-related antigen array	3	<20 min	Human serum; 3 patient samples & 3 controls	LED/CCD; Non-portable	Direct label-free
pi-RIfS [15]	antiphospholipid-syndrome-related antigen array	4	10 min	Human Serum; 41 patients samples & 24 controls; ELISA	CCD; Non-portable	Direct label-free
1-λ RIfS [16]	2D array of Salmonella LPS and CRP antibody	2	<4 min for CRP, <8 min for bacteria	Chicken sera	470 nm LED/photodiode; Portable	Direct label-free
Imaging 1-λ RIfS [17]	5 × 7 spots array of kinase inhibitors	5	Few min	Kinase model samples	535 nm LED; CCD; Non portable	Direct label-free
WLRS [20]	Spatially distinct antibody (CRP, d-Dimer) bands	2 (up to 7)	45 min	35 human plasma samples; clinical lab comparison	x-scan; Non portable	CRP direct; D-dimer two-site immunoassay with biotinylated reporter antibody and streptavidin
WLRS [21]	Spatially distinct antigen-protein conjugates bands	2	12 min	Spiked water samples	x-scan; Non portable	Competitive immunoassay; Secondary Ab amplification
MARS/ WLRS [22]	Multi-thickness WLRS chips coated with antigen-protein conjugates	2	12 min	Wheat/maize extracts	Dual-area spectral deconvolution; PoN-oriented	Competitive immunoassay; Secondary Ab amplification
AIR [23]	Cytokine antibody array	3	60 min	Not reported; Buffer; human serum	CCD; non-portable	Direct label-free
AIR [25]	Cytokine antibody microarray	14	Not reported	Not reported; Buffer	AIR reader; non-portable	Direct label-free
AIR [26]	Influenza serology 16 recombinant antigens array	3	60 min	13 field-collected mallard serum samples	AIR reader; non portable	Direct label-free
AIR [27]	Autoantigen array	5	Overnight	Not reported; 5 positive + 10 healthy donors	AIR, CCD; non-portable	Direct label-free

Table 1. *Cont.*

Platform [Ref.]	Multiplexing Format	Number of Targets	Assay Time	Sample/Validation	Detection Mode/Portability	Direct Detection/ Signal Amplification
AIR [28]	Aptamer arrays against thrombin and TGF-β1	2	Overnight	Buffer	AIR reader; non portable	Direct label-free
AIR [29]	Viral antigen probes for SARS-CoV-2, SARS-CoV-1, MERS-CoV	15	Overnight	Serum samples from 15 convalescent COVID-19 patients	ZIVA; Partially portable	Direct label-free
AIR [30]	Staphylococcus aureus serology	8	Overnight	82 patients with S. aureus infections and 30 healthy individuals	ZIVA; Partially portable	Secondary Ab amplification
AIR [31]	Glycan microarrays for influenza viruses	>100	Not reported	Buffer	AIR reader; non portable	Direct label-free
AIR [32]	Antigens array MERS, SARS-CoV-1, and SARS-CoV-2	2 RSV and 17 influenza A and B antigens	1 h	Human blood samples	ZIVA; Partially portable	Direct label-free
AIR [33]	25	25 (6 cytokines and 19 S. aureus-specific antibodies)	Overnight	429 human sera (401 analyzed)	ZIVA; Partially portable	Direct label-free
IRIS [36]	Antibody array against vesicular stomatitis virus (VSV)	3 proteins	0.5–18.5 h	VSV infected lysate	IRIS, CCD; non-portable	Direct label-free; fluorescence-based confirmatory assay
IRIS [37]	Antibody array against Fumonisin B1	20	40 min	Fumonisin B1 in buffer	IRIS, LED/CMOS; non-portable	Direct label-free
SP-IRIS [39]	Probes against the exosomal tetraspanins	3 markers	Overnight	Exosomes in buffer + human CSF	SP-IRIS counting; non-portable	Direct label-free
SP-IRIS [40]	DNA-directed antibody array against 3 recombinant vesicular stomatitis virus (rVSV) models	3	~60 min	rVSV models in buffer	SP-IRIS digital counting; Cartridge/PoC oriented	Direct label-free

Table 1. *Cont.*

Platform [Ref.]	Multiplexing Format	Number of Targets	Assay Time	Sample/Validation	Detection Mode/Portability	Direct Detection/ Signal Amplification
SP-IRIS [41]	Tetraspanin chips targeting extracellular vesicles in neurological disease	5	Not reported	19 patient samples + 10 healthy controls	ExoView R200+; Automated	Mixed; fluorescence labelling for phenotyping
SP-IRIS [42]	Capture antibody array against extracellular vesicles from human adipose tissue (adipo-chip)	5	Overnight	26 samples/13 donors	ExoView R200+; Automated	Mixed; fluorescence labelling for phenotyping
MP-IRIS [44]	DNA hybridization array	Multiple DNA stands	Real-time; Not reported total	Synthetic DNA proof-of-concept	Dual-wavelength MP-IRIS; non-portable	Direct label-free
MZI [46]	Allergen spotted integrated BB-MZI s	2	20 min	Buffer	BB-MZIs chips + external spectrometer; Partially portable	Direct label-free
MZI [47]	Allergen spotted integrated BB-MZI s	4	10 min pre-incubation + 6.5 min assay	Dairy industry rinsing water; ELISA	BB-MZIs chips + external spectrometer; Partially portable	Secondary Ab amplification
MZI [48]	Mycotoxin-protein conjugates spotted integrated BB-MZIs	3	12 min	29 Beers; ELISA/LC-MS/MS	BB-MZIs chips + external spectrometer; Partially portable	Secondary Ab amplification
MZI [49]	Integrated BB-MZIs spotted with Bacteria LPS	2	10 min water/15 min milk	Water/milk	10 BB-MZIs; Partial	Biotinylated secondary antibody and streptavidin
MZI [50]	All-in-one chip with 10 BB-MZIs spotted with antigens	3 allergens/2 mycotoxins	10/15 min	Rinsing water/beer	Fully integrated chip with 10 B-MZIs; Portable/automated	Secondary Ab amplification
MZI [51]	4 slot-waveguide MZIs spotted with synthetic miRNA	2 miRNAs	15 min	Urine; 3 cancer patients + 2 controls	Si_3N_4 MZI + InGaAs camera; portable	Direct label free

Table 1. *Cont.*

Platform [Ref.]	Multiplexing Format	Number of Targets	Assay Time	Sample/Validation	Detection Mode/Portability	Direct Detection/ Signal Amplification
aMZI [52]	6 sensing + 2 auxiliary aMZI spotted with SARS-CoV-2 proteins	3	Not reported	23 positive + 14 negative human plasma samples	Si_3N_4 waveguides, VCSEL detection; PoC-oriented	Direct Label-free; optional IgG amplification
BiMW [55]	Waveguides spotted with antibodies against respiratory Syncytial Virus nucleoproteins	-	9 min	Buffer	CMOS-fabricated chips; PoC-oriented	Direct Label-free
SPRi [63]	12-spot array of antibodies against NGAL, IL-18 and RBP	3	~46 min	Urine; 2 patients with acute kidney injury + 1 control	Smartphone SPRi; Portable	Sandwich immunoassay with antibody-functionalized magnetic nanoparticles
SPRi [64]	anti-CA-125 and anti-mesothelin spots	2	Not reported	FBS	SPR imaging; non-portable	Sandwich immunoassay with antibody-functionalized gold nanoparticles
SPRi [65]	array of antibodies against 4 prostate cancer biomarkers	4	~60 min	Buffer	SPR imaging; non-portable	Sandwich immunoassay with antibody-functionalized magnetic nanoparticles
SPRi [66]	Array with protein conjugates of 6 pesticides	6	4 min	Crops; HPLC/LC-MS/MS	OpenPlex SPR; non-portable	Label-free competitive immunoassay
SPRi [67]	44-antibody array against cell-surface antigens	44	<20 min	5 cancer cell lines; flow cytometry	IBIS MX96; non-portable	Direct label-free
SPRi [68]	Antibody & lectin array for circulating extracellular vesicles profiling	25	~15 min	71 type 2 diabetes mellitus + 47 hypertension patients+ 18 healthy controls	OpenPlex; Reusable, non-portable	Direct label-free
SPRi [69]	Ligand array for extracellular vesicles	10	Not reported	19 stroke patients + 20 healthy controls	XelPleX; non-portable	Mixed; gold-labeled secondary Abs

Multiplexing represents another important dimension of platform performance, although its implementation varies considerably across sensor architectures. AIR and SPRi primarily rely on spatially arranged arrays, enabling the simultaneous interrogation of multiple capture regions and supporting broad serological, biomarker and phenotypic

profiling. MZI and BiMW systems typically achieve multiplexing through the integration of multiple interferometric sensors, each functionalized with a distinct recognition element, offering a direct route toward compact, multianalyte photonic devices. IRIS combines spatial multiplexing with imaging-based readout and, in SP-IRIS configurations, single-particle counting and phenotyping. This extends the analytical capabilities beyond target quantification to include particle-level characterization and kinetic information. RIfS employs several strategies, including simultaneous imaging, sequential interrogation of spatially separated sensing regions, and array-based screening, whereas WLRS generally operates at lower levels of multiplexing, using sequentially addressed or spectrally resolved sensing areas. Thus, multiplexing capacity should be evaluated not only in terms of the number of analytes detected, but also in terms of the spatial, kinetic and phenotypic information generated.

Assay speed and system integration provide further criteria for differentiating these platforms. Several systems have already demonstrated portable or point-of-care/point-of-need (POC/PON) oriented operation, moving beyond the prospective potential for POC/PON applications. WLRS has been implemented in rapid POC/PON assays [20,22] while PD-IRIS was specifically developed to simplify single-particle virus detection for POC use [43]. SPRi has also been coupled to smartphone-based optical readout for POC application [63]. MZI platforms have pursued simplified and integrated operation, with the ultimate all-in-one configuration that integrates light sources, spectral analyzers and detector arrays on a single chip, thereby removing the need for external optical components [50]. RIfS has likewise demonstrated a portable single-wavelength detection module [16], while AIR has progressed toward automated cartridge-based workflows [32]. In this context, decentralized operation depends not merely on reducing assay time, but also on integrating or simplifying optical, fluidic, computational and sample-handling functions to establish a streamlined analytical workflow.

The types of samples used for validation further distinguish these technologies. The reviewed platforms have been evaluated in clinical biofluids, food products, environmental samples and veterinary specimens. AIR has been applied to relatively large human cohorts, particularly in multiplex serological and infection-related applications [30,33]. MZI, BiMW, and WLRS have also been repeatedly evaluated across diverse matrices including serum, plasma, urine, milk, beer, industrial rinsing water, and environmental water samples. SPRi has further strengthened its clinical relevance through multiplexed extracellular-vesicle profiling in defined patient cohorts [68,69], while IRIS has extended single-particle and EV analysis to clinically derived biofluids [39]. RIfS combines selected clinical validation with veterinary applications [17]. However, the level of evidence provided by these studies is not equivalent. Some platforms have been evaluated directly using minimally processed samples and benchmarked against established analytical or diagnostic methods, whereas others still rely on purified fractions, isolated vesicles, spiked matrices, or relatively small cohorts. Future evaluations should therefore prioritize the direct analysis of samples, independent validation using larger and more diverse sample sets, and systematic assessment of matrix effects and sample-preparation requirements. These factors are essential for determining whether performance achieved under controlled experimental conditions can be retained in practical applications.

The performance of label-free optical biosensors also depends on factors beyond the optical transducer itself, particularly the surface chemistry and processing steps that govern target capture, background suppression, and signal stability. Surface functionalization and blocking are critical across all platforms, especially in multiplexed assays, where nonspecific adsorption and cross-reactivity can compromise measurement reliability. WLRS studies illustrate this dependence particularly clearly by investigating antibody immobilization,

orientation, regeneration, and long-term surface stability as key performance parameters variables in their own right [70]. IRIS demonstrates a complementary approach to improving robustness through optical correction of bulk refractive-index variations and background-thickness effects, as illustrated by the dual-wavelength MP-IRIS configuration [44]. In MZI, BiMW, and SPRi systems, high analytical sensitivity or enhanced information content is frequently supported by secondary amplification, particle-based enhancement or preconcentration steps. Although these approaches can improve analytical performance, they may also increase assay complexity. RIfS, meanwhile, encompasses both porous and planar architectures, which exhibit distinct sources of signal variation and consequently require different approaches to surface and optical control [13,14]. Accordingly, optimization strategies should address reproducible surface preparation, resistance to matrix-induced background signals, long-term stability and simplification of assay workflows, rather than focusing on lower detection limits alone.

Taken together, the available literature does not point to a single optimal architecture for label-free multiplexed optical biosensing, but rather highlights different combinations of analytical and engineering capabilities suited to specific applications. High-density multiplexing, photonic integration, rapid analysis, single-particle resolution, and compatibility with complex samples are distributed unevenly across the platforms, and improvements in one performance dimension may introduce additional requirements or trade-offs in another. Consequently, meaningful comparisons should not rely on a single performance metric, but should instead consider how effectively each system combines analytical sensitivity and information content with sample compatibility, assay simplicity, robustness and the requirements of the intended application. Across the field, the transition from proof-of-concept demonstrations toward practical implementation increasingly depends on direct evaluation using complex samples, reduced reliance on external instrumentation and additional processing steps, effective control of surface and matrix effects, and validation using sufficiently large and diverse sample sets. Future advances are therefore likely to depend not simply on further reductions in detection limits, but on the successful integration of these requirements into reproducible and robust systems designed to meet the demands of specific analytical applications.

It should be noted that, although this review focuses on the analysis and comparison of seven optical biosensing platforms with multiplexing capabilities, other optical sensing strategies, such as surface-enhanced Raman scattering (SERS) [2,3] and paper-based biosensors [4,5], are also increasingly being explored for a wide range of analytical applications, including multiplexed analyte detection.

4. Conclusions

Label-free optical biosensors encompass a diverse range of platforms that differ in their analytical sensitivity, multiplexing capabilities, integration potential, and sample compatibility. Their performance cannot be assessed solely on the basis of detection limits, as the type of information generated, assay design, sample matrix, and degree of system integration also determine their suitability for specific applications. AIR and SPRi platforms support spatial multiplexing, whereas IRIS enables imaging-based analysis and single-particle detection. MZI and BiMW systems, in contrast, are particularly well suited to photonic integration. WLRS and RIfS further illustrate the versatility of reflectometric approaches across a broad range of analytical applications. These differences highlight that no single platform is optimal for all applications. Platform selection should instead be guided by the required analytical performance, assay complexity, the nature of the sample, and the practical constraints of the measurement system. Further advances will depend on more extensive validation using complex samples, improved control of surface-related and

matrix effects, and reduced dependence on external instrumentation and additional sample-processing steps. Beyond improvements in analytical sensitivity, addressing these challenges will be essential for achieving more reproducible, robust, and practically deployable label-free optical biosensing systems.

Author Contributions: Conceptualization, M.D.D., D.T., I.R., K.G.B. and P.P.; writing—original draft preparation, M.D.D., D.T., K.G.B. and P.P.; writing—review and editing, I.R., E.R., K.G.B. and P.P.; visualization, M.D.D., D.T., I.R., E.R., K.G.B. and P.P.; supervision, I.R., E.R., K.G.B. and P.P. All authors have read and agreed to the published version of the manuscript.

Funding: This research received no external funding.

Institutional Review Board Statement: Not applicable.

Informed Consent Statement: Not applicable.

Data Availability Statement: No new data were created or analyzed in this study.

Conflicts of Interest: The authors declare no conflicts of interest.

Abbreviations

The following abbreviations are used in this manuscript:

RIfS	Reflectometric Interference Spectroscopy
WLRS	White Light Reflectance Spectroscopy
AIR	Arrayed Imaging Reflectometry
IRIS	Interferometric Reflectance Imaging Sensor
MZIs	Mach–Zehnder Interferometers
BiMW	Bimodal Interferometers
SPR	Surface Plasmon Resonance
SPRi	Surface Plasmon Resonance Imaging
UV/vis	Ultra Violet/visible
LED	Light Emitting Diode
NAA	Nanoporous anodic alumina
ΔEOT	Differential Effective Optical Thickness
CCD	Charge-Coupled Device
pi-RIfS	Polarized Imaging Reflectometric Interference Spectroscopy
PDMS	Polydimethylsiloxane
BSA	Bovine serum Albumin
11-AUTMS	11-Amino-undecyltrimethoxysilane
NHS	N-Hydroxysuccinimide
DIC	Diisopropylcarbodiimide
IgG	Immunoglobulin G
ELISA	Enzyme immunoassay
GOPTS	3-Glycidyloxypropyltrimethoxysilane
CRP	C-Reactive Protein
APTES	3-Amino-propyltriethoxysilane
MARS	Multi-Area Reflectance Spectroscopy
ToF-SIMS	Time-of-Flight Secondary Ion Mass Spectrometry
TF	Tissue Factor
PEG	Polyethylene glycol
IgM	Immunoglobulin M
FBS	Fetal Bovine Serum
PFU	Plaque-Forming Units
HRP	Horse Radish Peroxidase
DAB	3,3′-Diaminobenzidine
AUC	Area Under the Curve
CMOS	Complementary Metal–Oxide–Semiconductor
VSV	Vesicular Stomatitis Virus
SP-IRIS	Single-Particle Interferometric Reflectance Imaging Sensor

rVSV	Recombinant Vesicular Stomatitis Virus
EV	Extracellular Vesicle
CSF	Cerebrospinal Fluid
RRMS	Relapsing-Remitting Multiple Sclerosis
PPMS	Primary Progressive Multiple Sclerosis
PD-IRIS	Pixel-Diversity Interferometric Reflectance Imaging Sensor
MPXV	Monkeypox Virus
MP-IRIS	Multi-Parametric Interferometric Reflectance Imaging Sensor
RIU	Refractive Index Units
BB-MZI	Broad-Band Mach–Zehnder Interferometer
AFB1	Aflatoxin B1
FB1	Fumonisin B1
DON	Deoxynivalenol
LPS	Lipopolysaccharide
CFU	Colony-Forming Units
aMZI	Asymmetric Mach–Zehnder Interferometer
VCSEL	Vertical-Cavity Surface-Emitting Laser
EDC	1-Ethyl-3-(3-dimethylaminopropyl)carbodiimide
RSV	Respiratory Syncytial Virus
AKI	Acute Kidney Injury
T2DM	Type 2 Diabetes Mellitus
HT	Hypertension
POC	Point-of-care
PON	Point-of-need
ssDNA	single-stranded DNA
SERS	surface-enhanced Raman scatterin

References

1. Singh, A.K.; Mittal, S.; Das, M.; Saharia, A.; Tiwari, M. Optical Biosensors: A Decade in Review. *Alex. Eng. J.* **2023**, *67*, 673–691. [CrossRef]
2. Zhao, Y.; Xu, Y.; Jing, X.; Ma, W. SERS-active plasmonic metal NP-CsPbX3 films for multiple veterinary drug residues detection. *Food Chem.* **2023**, *412*, 135420. [CrossRef] [PubMed]
3. Liang, D.; Xu, Y.; Peng, F.; Ma, W.; Zhao, Y. Plasmonic metal NP-bismuth composite film with amplified SERS activity for multiple detection of pesticides and veterinary drugs. *Chem. Eng. J.* **2023**, *474*, 145933. [CrossRef]
4. Li, J.; Chen, K.; Su, Y.; Zhu, L.-J.; Zhang, H.; Xu, W.-T.; Li, X.-Y. Paper-Based Biosensors Based on Multiple Recognition Modes for Visual Detection of Microbially Contaminated Food. *J. Future Foods* **2024**, *4*, 61–70. [CrossRef]
5. Kumari, S.; Islam, M.; Gupta, A. Paper-based multiplex biosensors for inexpensive healthcare diagnostics: A comprehensive review. *Biomed. Microdevices* **2023**, *25*, 17. [CrossRef] [PubMed]
6. Angelopoulou, M.; Kakabakos, S.; Petrou, P. Label-Free Biosensors Based onto Monolithically Integrated onto Silicon Optical Transducers. *Chemosensors* **2018**, *6*, 52. [CrossRef]
7. Fechner, P.; Gauglitz, G.; Proll, G. Through the Looking-Glass—Recent Developments in Reflectometry Open New Possibilities for Biosensor Applications. *TrAC—Trends Anal. Chem.* **2022**, *156*, 116708. [CrossRef]
8. Jha, R.; Gorai, P.; Shrivastav, A.; Pathak, A. Label-Free Biochemical Sensing Using Processed Optical Fiber Interferometry: A Review. *ACS Omega* **2024**, *9*, 3037–3069. [CrossRef] [PubMed]
9. Kozma, P.; Kehl, F.; Ehrentreich-Förster, E.; Stamm, C.; Bier, F.F. Integrated Planar Optical Waveguide Interferometer Biosensors: A Comparative Review. *Biosens. Bioelectron.* **2014**, *58*, 287–307. [CrossRef] [PubMed]
10. Casquel, R.; Holgado, M.; Laguna, M.F.; Hernández, A.L.; Santamaría, B.; Lavín, Á.; Tramarin, L.; Herreros, P. Engineering Vertically Interrogated Interferometric Sensors for Optical Label-Free Biosensing. *Anal. Bioanal. Chem.* **2020**, *412*, 3285–3297. [CrossRef] [PubMed]
11. Proll, G.; Steinle, L.; Pröll, F.; Kumpf, M.; Moehrle, B.; Mehlmann, M.; Gauglitz, G. Potential of Label-Free Detection in High-Content-Screening Applications. *J. Chromatogr. A* **2007**, *1161*, 2–8. [CrossRef] [PubMed]
12. Proll, G.; Markovic, G.; Fechner, P.; Proell, F.; Gauglitz, G. Reflectometric Interference Spectroscopy. In *Biosensors and Biodetection: Methods and Protocols, Volume 1: Optical-Based Detectors*; Rasooly, A., Prickril, B., Eds.; Springer Science and Business Media LLC: Berlin/Heidelberg, Germany, 2017; Volume 1571, pp. 207–220.
13. Cantons, J.M.; Formentin, P.; Ferré-Borrull, J.; Bachhuka, A.; Marsal, L.F. Structural Nanoengineering of Modulated Structures Based on Nanoporous Anodic Alumina for Biosensing Applications. *Adv. Sens. Res.* **2026**, *5*, 70161. [CrossRef]

14. Bleher, O.; Schindler, A.; Yin, M.X.; Holmes, A.B.; Luppa, P.B.; Gauglitz, G.; Proll, G. Development of a New Parallelized, Optical Biosensor Platform for Label-Free Detection of Autoimmunity-Related Antibodies Multiplex Platforms in Diagnostics and Bioanalytics. *Anal. Bioanal. Chem.* **2014**, *406*, 3305–3314. [CrossRef] [PubMed]
15. Schindler, A.R.; Bleher, O.; Thaler, M.A.; Kocot, C.J.; Steigerwald, U.; Proll, G.; Gauglitz, G.; Luppa, P.B. Diagnostic Performance Study of an Antigen Microarray for the Detection of Antiphospholipid Antibodies in Human Serum. *Clin. Chem. Lab. Med.* **2015**, *53*, 801–808. [CrossRef] [PubMed]
16. Ewald, M.; Fechner, P.; Gauglitz, G. A Multi-Analyte Biosensor for the Simultaneous Label-Free Detection of Pathogens and Biomarkers in Point-of-Need Animal Testing. *Anal. Bioanal. Chem.* **2015**, *407*, 4005–4013. [CrossRef] [PubMed]
17. Wurster, V.; Fechner, P.; Proll, G.; Pamies-Cuberos, R.; Frech, M.; Baumgärtner, J.; Malissa, A.; Marchetti-Deschmann, M.; Ivleva, N.P.; Saal, C.; et al. Reflectometric-Based Sensor Arrays for the Screening of Kinase-Inhibitor Interactions and Kinetic Determination. *Anal. Bioanal. Chem.* **2025**, *417*, 6811–6822. [CrossRef] [PubMed]
18. Koukouvinos, G.; Petrou, P.; Goustouridis, D.; Misiakos, K.; Kakabakos, S.; Raptis, I. Development and Bioanalytical Applications of a White Light Reflectance Spectroscopy Label-Free Sensing Platform. *Biosensors* **2017**, *7*, 46. [CrossRef] [PubMed]
19. Karachaliou, C.E.; Koukouvinos, G.; Goustouridis, D.; Raptis, I.; Kakabakos, S.; Livaniou, E.; Petrou, P. Recent Developments in the Field of Optical Immunosensors Focusing on a Label-Free, White Light Reflectance Spectroscopy-Based Immunosensing Platform. *Sensors* **2022**, *22*, 5114. [CrossRef] [PubMed]
20. Koukouvinos, G.; Petrou, P.; Misiakos, K.; Drygiannakis, D.; Raptis, I.; Stefanitsis, G.; Martini, S.; Nikita, D.; Goustouridis, D.; Moser, I.; et al. Simultaneous Determination of CRP and D-Dimer in Human Blood Plasma Samples with White Light Reflectance Spectroscopy. *Biosens. Bioelectron.* **2016**, *84*, 89–96. [CrossRef] [PubMed]
21. Stavra, E.; Petrou, P.S.; Koukouvinos, G.; Kiritsis, C.; Pirmettis, I.; Papadopoulos, M.; Goustouridis, D.; Economou, A.; Misiakos, K.; Raptis, I.; et al. Simultaneous Determination of Paraquat and Atrazine in Water Samples with a White Light Reflectance Spectroscopy Biosensor. *J. Hazard. Mater.* **2018**, *359*, 67–75. [CrossRef] [PubMed]
22. Anastasiadis, V.; Koukouvinos, G.; Petrou, P.S.; Economou, A.; Dekker, J.; Harjanne, M.; Heimala, P.; Goustouridis, D.; Raptis, I.; Kakabakos, S.E. Multiplexed Mycotoxins Determination Employing White Light Reflectance Spectroscopy and Silicon Chips with Silicon Oxide Areas of Different Thickness. *Biosens. Bioelectron.* **2020**, *153*, 112035. [CrossRef] [PubMed]
23. Mace, C.R.; Striemer, C.C.; Miller, B.L. Detection of Human Proteins Using Arrayed Imaging Reflectometry. *Biosens. Bioelectron.* **2008**, *24*, 334–337. [CrossRef] [PubMed]
24. Kosoy, G.; Miller, B.L. Two Decades of Arrayed Imaging Reflectometry for Sensitive, High-Throughput Biosensing. *Biosensors* **2023**, *13*, 870. [CrossRef] [PubMed]
25. Carter, J.A.; Mehta, S.D.; Mungillo, M.V.; Striemer, C.C.; Miller, B.L. Analysis of Inflammatory Biomarkers by Arrayed Imaging Reflectometry. *Biosens. Bioelectron.* **2011**, *26*, 3944–3948. [CrossRef] [PubMed]
26. Bucukovski, J.; Latorre-Margalef, N.; Stallknecht, D.E.; Miller, B.L. A Multiplex Label-Free Approach to Avian Influenza Surveillance and Serology. *PLoS ONE* **2015**, *10*, e0134484. [CrossRef] [PubMed]
27. Bucukovski, J.; Carter, J.A.; Striemer, C.C.; Müllner, S.; Schulte-Pelkum, J.; Schulz-Knappe, P.; Miller, B.L. Label-Free Microarray-Based Detection of Autoantibodies in Human Serum. *J. Immunol. Methods* **2018**, *459*, 44–49. [CrossRef] [PubMed]
28. Klose, A.M.; Miller, B.L. A Stable Biotin–Streptavidin Surface Enables Multiplex, Label-Free Protein Detection by Aptamer and Aptamer–Protein Arrays Using Arrayed Imaging Reflectometry. *Sensors* **2020**, *20*, 5745. [CrossRef] [PubMed]
29. Steiner, D.J.; Cognetti, J.S.; Luta, E.P.; Klose, A.M.; Bucukovski, J.; Bryan, M.R.; Schmuke, J.J.; Nguyen-Contant, P.; Sangster, M.Y.; Topham, D.J.; et al. Array-Based Analysis of SARS-CoV-2, Other Coronaviruses, and Influenza Antibodies in Convalescent COVID-19 Patients. *Biosens. Bioelectron.* **2020**, *169*, 112643. [CrossRef] [PubMed]
30. Klose, A.M.; Daiss, J.L.; Ho, L.; Beck, C.A.; Striemer, C.C.; Muthukrishnan, G.; Miller, B.L. StaphAIR: A Label-Free Antigen Microarray Approach to Detecting Anti-Staphylococcus Aureus Antibody Responses in Orthopedic Infections. *Anal. Chem.* **2021**, *93*, 13580–13588. [CrossRef] [PubMed]
31. Zhang, H.; Klose, A.M.; Miller, B.L. Label-Free, Multiplex Glycan Microarray Biosensor for Influenza Virus Detection. *Bioconjugate Chem.* **2021**, *32*, 533–540. [CrossRef] [PubMed]
32. Klose, A.M.; Kosoy, G.; Miller, B.L. Arrayed Imaging Reflectometry Monitoring of Anti-Viral Antibody Production throughout Vaccination and Breakthrough Covid-19. *PLoS ONE* **2023**, *18*, e0277846. [CrossRef] [PubMed]
33. Klose, A.M.; Beck, C.A.; Kates, S.L.; Muthukrishnan, G.; Schwarz, E.M.; Miller, B.L. Dual-Scale StaphAIR: Predictive Modeling for the Diagnosis of *S. aureus* Infection via Simultaneous Detection and Quantification of Cytokines and Antibodies. *Anal. Chem.* **2026**, *98*, 15599–15608. [CrossRef] [PubMed]
34. Avci, O.; Ünlü, N.L.; Özkumur, A.Y.; Ünlü, M.S. Interferometric Reflectance Imaging Sensor (IRIS)—A Platform Technology for Multiplexed Diagnostics and Digital Detection. *Sensors* **2015**, *15*, 17649–17665. [CrossRef] [PubMed]
35. Bakhshpour-Yucel, M.; Unlu, N.L.; Seymour, E.; Denizli, A. A Comprehensive Review of Interferometric Reflectance Imaging Sensor as a Sensitive Detection Platform and Its Application Areas. *Biosens. Bioelectron. X* **2025**, *22*, 100574. [CrossRef]

36. Lopez, C.A.; Daaboul, G.G.; Vedula, R.S.; Özkumur, E.; Bergstein, D.A.; Geisbert, T.W.; Fawcett, H.E.; Goldberg, B.B.; Connor, J.H.; Ünlü, M.S. Label-Free Multiplexed Virus Detection Using Spectral Reflectance Imaging. *Biosens. Bioelectron.* **2011**, *26*, 3432–3437. [CrossRef] [PubMed]
37. Chiodi, E.; Marn, A.M.; Geib, M.T.; Ekiz Kanik, F.; Rejman, J.; Ankrapp, D.; Ünlü, M.S. Highly Multiplexed Label-Free Imaging Sensor for Accurate Quantification of Small-Molecule Binding Kinetics. *ACS Omega* **2020**, *5*, 25358–25364. [CrossRef] [PubMed]
38. Marn, A.M.; Needham, J.; Chiodi, E.; Ünlü, M.S. Multiplexed, High-Sensitivity Measurements of Antibody Affinity Using Interferometric Reflectance Imaging Sensor. *Biosensors* **2021**, *11*, 483. [CrossRef] [PubMed]
39. Daaboul, G.G.; Gagni, P.; Benussi, L.; Bettotti, P.; Ciani, M.; Cretich, M.; Freedman, D.S.; Ghidoni, R.; Ozkumur, A.Y.; Piotto, C.; et al. Digital Detection of Exosomes by Interferometric Imaging. *Sci. Rep.* **2016**, *6*, 37246. [CrossRef] [PubMed]
40. Seymour, E.; Ünlü, N.L.; Carter, E.P.; Connor, J.H.; Ünlü, M.S. Configurable Digital Virus Counter on Robust Universal DNA Chips. *ACS Sens.* **2021**, *6*, 229–237. [CrossRef] [PubMed]
41. Bravo-Miana, R.D.C.; Arizaga-Echebarria, J.K.; Sabas-Ortega, V.; Crespillo-Velasco, H.; Prada, A.; Castillo-Triviño, T.; Otaegui, D. Tetraspanins, GLAST and L1CAM Quantification in Single Extracellular Vesicles from Cerebrospinal Fluid and Serum of People with Multiple Sclerosis. *Biomedicines* **2024**, *12*, 2245. [CrossRef] [PubMed]
42. Lago-Baameiro, N.; Camino, T.; Estévez-López, A.; Vázquez-Durán, A.; Fernández-Nogueira, M.; Sueiro, A.; Santos, F.; Baltar, J.; Pardo, M. Design of a Single Particle-Interferometric Reflectance Imaging Sensor Adipo-Chip for Obesity Biomarker Screening. *Sci. Rep.* **2025**, *15*, 38160. [CrossRef] [PubMed]
43. Aslan, M.; Seymour, E.; Brickner, H.; Clark, A.E.; Celebi, I.; Townsend, M.B.; Satheshkumar, P.S.; Riley, M.; Carlin, A.F.; Ünlü, M.S.; et al. A Label-Free Optical Biosensor-Based Point-of-Care Test for the Rapid Detection of Monkeypox Virus. *Biosens. Bioelectron.* **2025**, *269*, 116932. [CrossRef] [PubMed]
44. Aslan, M.; Snekvik, S.; Seymour, E.; Gür, S.D.; Ergene, E.; Ünlü, N.L.; Ünlü, M.S. Multi-Parametric Interferometric Reflectance Imaging Sensor. *Sci. Rep.* **2026**, *16*, 10780. [CrossRef] [PubMed]
45. Psarouli, A.; Salapatas, A.; Botsialas, A.; Petrou, P.S.; Raptis, I.; Makarona, E.; Jobst, G.; Tukkiniemi, K.; Sopanen, M.; Stoffer, R.; et al. Monolithically Integrated Broad-Band Mach-Zehnder Interferometers for Highly Sensitive Label-Free Detection of Biomolecules through Dual Polarization Optics. *Sci. Rep.* **2015**, *5*, 17600. [CrossRef] [PubMed]
46. Psarouli, A.; Botsialas, A.; Salapatas, A.; Stefanitsis, G.; Nikita, D.; Jobst, G.; Chaniotakis, N.; Goustouridis, D.; Makarona, E.; Petrou, P.S.; et al. Fast Label-Free Detection of C-Reactive Protein Using Broad-Band Mach-Zehnder Interferometers Integrated on Silicon Chips. *Talanta* **2017**, *165*, 458–465. [CrossRef] [PubMed]
47. Angelopoulou, M.; Petrou, P.S.; Makarona, E.; Haasnoot, W.; Moser, I.; Jobst, G.; Goustouridis, D.; Lees, M.; Kalatzi, K.; Raptis, I.; et al. Ultrafast Multiplexed-Allergen Detection through Advanced Fluidic Design and Monolithic Interferometric Silicon Chips. *Anal. Chem.* **2018**, *90*, 9559–9567. [CrossRef] [PubMed]
48. Pagkali, V.; Petrou, P.S.; Makarona, E.; Peters, J.; Haasnoot, W.; Jobst, G.; Moser, I.; Gajos, K.; Budkowski, A.; Economou, A.; et al. Simultaneous Determination of Aflatoxin B1, Fumonisin B1 and Deoxynivalenol in Beer Samples with a Label-Free Monolithically Integrated Optoelectronic Biosensor. *J. Hazard. Mater.* **2018**, *359*, 445–453. [CrossRef] [PubMed]
49. Angelopoulou, M.; Petrou, P.; Misiakos, K.; Raptis, I.; Kakabakos, S. Simultaneous Detection of *Salmonella typhimurium* and *Escherichia coli O157:H7* in Drinking Water and Milk with Mach–Zehnder Interferometers Monolithically Integrated on Silicon Chips. *Biosensors* **2022**, *12*, 507. [CrossRef] [PubMed]
50. Angelopoulou, M.; Pagkali, V.; Makarona, E.; Misiakos, K.; Raptis, I.; Petrou, P.; Kakabakos, S.; Peters, J.; Jobst, G.; Goustouridis, D.; et al. Multiplexed Detection of Food Contaminants with a Portable Reader Based on All-in-One Monolithic Photonic Chips. *Opt. Laser Technol.* **2024**, *177*, 111192. [CrossRef]
51. Liu, Q.; Shin, Y.; Kee, J.S.; Kim, K.W.; Mohamed Rafei, S.R.; Perera, A.P.; Tu, X.; Lo, G.Q.; Ricci, E.; Colombel, M.; et al. Mach-Zehnder Interferometer (MZI) Point-of-Care System for Rapid Multiplexed Detection of MicroRNAs in Human Urine Specimens. *Biosens. Bioelectron.* **2015**, *71*, 365–372. [CrossRef] [PubMed]
52. Besselink, G.; Schütz-Trilling, A.; Veerbeek, J.; Verbruggen, M.; van der Meer, A.; Schonenberg, R.; Dam, H.; Evers, K.; Lindhout, E.; Garritsen, A.; et al. Asymmetric Mach–Zehnder Interferometric Biosensing for Quantitative and Sensitive Multiplex Detection of Anti-SARS-CoV-2 Antibodies in Human Plasma. *Biosensors* **2022**, *12*, 553. [CrossRef] [PubMed]
53. Zinoviev, K.E.; Gonzalez-Guerrero, A.B.; Dominguez, C.; Lechuga, L.M. Integrated Bimodal Waveguide Interferometric Biosensor for Label-Free Analysis. *J. Light. Technol.* **2011**, *29*, 1926–1930. [CrossRef]
54. Torrijos-Morán, L.; Lisboa, B.D.; Soler, M.; Lechuga, L.M.; García-Rupérez, J. Integrated optical bimodal waveguide biosensors: Principles and applications. *Results Opt.* **2022**, *9*, 100285. [CrossRef]
55. Alonso-Fernández, A.; Ramírez-Priego, P.; Estévez, M.-C.; Fernández-Gavela, A.; Lechuga, L.M. Scaling Nanophotonic Interferometric Biosensors toward Parallel Detection of Multiple Biomarkers. *ACS Sens.* **2026**, *11*, 6071–6079. [CrossRef] [PubMed]
56. Špringer, T.; Bocková, M.; Slabý, J.; Sohrabi, F.; Čapková, M.; Homola, J. Surface Plasmon Resonance Biosensors and Their Medical Applications. *Biosens. Bioelectron.* **2025**, *278*, 117308. [CrossRef] [PubMed]

57. Ravindran, N.; Kumar, S.; Yashini, M.; Rajeshwari, S.; Mamathi, C.A.; Thirunavookarasu, S.N.; Sunil, C.K. Recent Advances in Surface Plasmon Resonance (SPR) Biosensors for Food Analysis: A Review. *Crit. Rev. Food Sci. Nutr.* **2023**, *63*, 1055–1077. [CrossRef] [PubMed]
58. Olaru, A.; Bala, C.; Jaffrezic-Renault, N.; Aboul-Enein, H.Y. Surface Plasmon Resonance (SPR) Biosensors in Pharmaceutical Analysis. *Crit. Rev. Anal. Chem.* **2015**, *45*, 97–105. [CrossRef] [PubMed]
59. Wang, Q.; Ren, Z.H.; Zhao, W.M.; Wang, L.; Yan, X.; Zhu, A.S.; Qiu, F.M.; Zhang, K.K. Research Advances on Surface Plasmon Resonance Biosensors. *Nanoscale* **2022**, *14*, 564–591. [CrossRef] [PubMed]
60. Puiu, M.; Bala, C. SPR and SPR Imaging: Recent Trends in Developing Nanodevices for Detection and Real-Time Monitoring of Biomolecular Events. *Sensors* **2016**, *16*, 870. [CrossRef] [PubMed]
61. Liu, C.; Hu, F.; Yang, W.; Xu, J.; Chen, Y. A Critical Review of Advances in Surface Plasmon Resonance Imaging Sensitivity. *TrAC—Trends Anal. Chem.* **2017**, *97*, 354–362. [CrossRef]
62. Xu, J.; Zhang, P.; Chen, Y. Surface Plasmon Resonance Biosensors: A Review of Molecular Imaging with High Spatial Resolution. *Biosensors* **2024**, *14*, 84. [CrossRef] [PubMed]
63. Zhang, Q.; Li, Y.; Hu, Q.; Xie, R.; Zhou, W.; Liu, X.; Wang, Y. Smartphone Surface Plasmon Resonance Imaging for the Simultaneous and Sensitive Detection of Acute Kidney Injury Biomarkers with Noninvasive Urinalysis. *Lab Chip* **2022**, *22*, 4941–4949. [CrossRef] [PubMed]
64. de Macedo, E.F.; Nascimento, L.S.; Hou, Y.; Mathey, R.; Tada, D.B. Simultaneous Detection of CA-125 and Mesothelin by Gold Nanoparticles in Surface Plasmon Resonance. *Sens. Biosens. Res.* **2024**, *43*, 100609. [CrossRef]
65. Ucak-Ozkaya, G.; Durak, M.Z.; Sharafeldin, M.; Rusling, J.F. Ultrasensitive Multiplexed Detection of Cancer Biomarker Proteins Using SPR Imaging. *Microchem. J.* **2025**, *216*, 114562. [CrossRef]
66. Miyake, S.; Hirakawa, Y.; Yamasaki, T.; Watanabe, E.; Harada, A.; Iwasa, S.; Narita, H. Simultaneous Detection of Six Different Types of Pesticides by an Immunosensor Based on Surface Plasmon Resonance. *Anal. Sci.* **2020**, *36*, 335–340. [CrossRef] [PubMed]
67. Stojanović, I.; Ruivo, C.F.; Van Der Velden, T.J.G.; Schasfoort, R.B.M.; Terstappen, L.W.M.M. Multiplex Label Free Characterization of Cancer Cell Lines Using Surface Plasmon Resonance Imaging. *Biosensors* **2019**, *9*, 70. [CrossRef] [PubMed]
68. Shibuta, T.; Takada, Y.; Nishinosono, S.; Yasuda, S.; Ono, Y.; Hirooka, Y.; Irikura, D.; Saito, K.; Umemura, T. Disease-Specific Signatures of Circulating Extracellular Vesicles Detected by the Surface Plasmon Resonance Imaging: A Pilot Study. *Extracell. Vesicles Circ. Nucleic Acids* **2025**, *6*, 36–53. [CrossRef] [PubMed]
69. Picciolini, S.; Mangolini, V.; Rodà, F.; Montesano, A.; Arnaboldi, F.; Liuzzi, P.; Mannini, A.; Bedoni, M.; Gualerzi, A. Multiplexing Biosensor for the Detection of Extracellular Vesicles as Biomarkers of Tissue Damage and Recovery after Ischemic Stroke. *Int. J. Mol. Sci.* **2023**, *24*, 7937. [CrossRef] [PubMed]
70. Gajos, K.; Sanocka, K.; Wytrwał, M.; Dąbczyński, P.; Budkowski, A. PH-Dependent Orientation of Physisorbed and Chemisorbed Antibodies on Silicon Determined with TOF-SIMS and Its Effect on in-Flow Capture Assay Monitored with WLRS Sensor. *Appl. Surf. Sci.* **2024**, *656*, 159644. [CrossRef]

Disclaimer/Publisher's Note: The statements, opinions and data contained in all publications are solely those of the individual author(s) and contributor(s) and not of MDPI and/or the editor(s). MDPI and/or the editor(s) disclaim responsibility for any injury to people or property resulting from any ideas, methods, instructions or products referred to in the content.